
A Theory of How Pretraining Shapes Inductive Bias in Fine-Tuning

Nicolás Anguita¹
Francesco Locatello² Andrew M. Saxe³ Marco Mondelli² Flavia Mancini¹
Samuel Lippel^{*4} Clémentine Dominé^{*2}

Abstract

Pretraining and fine-tuning are central stages in modern machine learning systems. In practice, feature learning plays an important role across both stages: deep neural networks learn a broad range of useful features during pretraining and further refine those features during fine-tuning. However, an end-to-end theoretical understanding of how choices of initialization impact the ability to reuse and refine features during fine-tuning has remained elusive. Here we develop an analytical theory of the pretraining–fine-tuning pipeline in diagonal linear networks, deriving exact expressions for the generalization error as a function of initialization parameters and task statistics. We find that different initialization choices place the network into four distinct fine-tuning regimes that are distinguished by their ability to support feature learning and reuse—and therefore by the task statistics for which they are beneficial. In particular, a smaller initialization scale in earlier layers enables the network to both reuse and refine its features, leading to superior generalization on fine-tuning tasks that rely on a subset of pretraining features. We demonstrate empirically that the same initialization parameters impact generalization in nonlinear networks trained on CIFAR-100. Overall, our results demonstrate analytically how data and network initialization interact to shape fine-tuning generalization, highlighting an important role for the relative scale of initialization across different layers in enabling continued feature learning during fine-tuning.

1. Introduction

Deep neural networks are often trained in stages: first, they are pretrained on general-purpose tasks for which large amounts of data are available; then, they are fine-tuned on the actual target task, for which data may be more limited. This pretraining–fine-tuning pipeline (PT+FT) has emerged as an essential workhorse for modern deep learning (Bommasani, 2021; Parthasarathy et al., 2024; Awais et al., 2025).

To benefit from fine-tuning, neural networks must learn task-specific features during pretraining and reuse them during fine-tuning (Lampinen & Ganguli, 2018; Saxe et al., 2019; Shachaf et al., 2021; Tahir et al., 2024). At the same time, fine-tuning further adapts these features, potentially improving generalization (Yosinski et al., 2014; Huh et al., 2016; Jain et al., 2023). As a result, the success of the PT+FT pipeline critically depends on how feature learning unfolds over the pretraining and fine-tuning stages.

Despite the practical success of PT+FT, the factors governing feature learning across pretraining and fine-tuning have remained unclear. Prior work has shown that weight initialization—in particular, its absolute and relative scale across layers—shifts neural network training between a fixed-feature (“lazy”) and a feature-learning (“rich”) regime (Chizat et al., 2019; Braun et al., 2022; Dominé et al., 2024; Kunin et al., 2024). In the single-task setting, feature-learning regimes often induce improved generalization (Chizat & Bach, 2020; Fort et al., 2020; Vyas et al., 2022). However, it remains unclear how these insights extend to multi-stage training regimes such as PT+FT, with only a few exceptions discussed further in Section 2 (Lippel & Lindsey, 2024). This limits our ability to use weight initialization as a principled tool for controlling the balance between reusing pretrained features and inducing continued feature learning. To address this gap, we study the PT+FT pipeline in diagonal linear networks, a tractable theoretical model that exhibits feature-learning behavior, and develop an end-to-end theory of the resulting generalization error. Our theory elucidates how weight initialization affects the inductive bias of PT+FT, and how this bias interacts with

Co-senior authors (marked with *). ¹Department of Engineering, University of Cambridge ²Institute of Science and Technology, Austria (ISTA) ³Gatsby Computational Neuroscience Unit and Sainsbury Wellcome Centre, UCL ⁴Center for Theoretical Neuroscience, Columbia University. Correspondence to: Nicolás Anguita <na658@cam.ac.uk>.

data properties to determine when different initialization schemes are optimal.

Specific Contributions.

- We analytically derive the implicit bias of PT+FT in diagonal linear networks and the resulting generalization error as a function of weight initialization, task parameters, and data scale (Section 4).
- We identify three limiting regimes induced by this implicit bias: (I) a pretraining-independent rich regime, (II) a pretraining-dependent lazy regime, and (III) a pretraining-independent lazy regime. We further highlight a universal trade-off between pretraining dependence and feature learning in fine-tuning (Section 5.1).
- In light of this trade-off, we highlight a fourth, intermediate learning regime: (IV) the pretraining-dependent rich regime. Notably, we find that the relative scale of initialization across layers plays a key role in entering this regime (Section 5.2).
- We demonstrate that pretraining and fine-tuning task parameters determine which of these regimes will generalize best (Section 5.3).
- Finally, in Section 6, we demonstrate that theoretical insights derived from simple networks extend to ResNets trained on CIFAR-100.

Altogether, we provide an end-to-end understanding of how initialization choices shape fine-tuning generalization. In doing so, we identify actionable levers for controlling the interplay between reusing pretrained features, refining those features, and learning new features.

2. Related Work

Rich and Lazy Learning. The distinction between lazy and rich learning regimes has become central to understanding how overparameterized neural networks learn and generalize. In the lazy regime, training dynamics are governed by a fixed representation, causing the network to effectively behave like a kernel machine (Jacot et al., 2018; Chizat et al., 2019). In contrast, the rich (or feature-learning) regime is marked by the emergence of task-specific representations and is commonly linked to finite-width networks and smaller weight scales (Saxe et al., 2013; Chizat & Bach, 2020; Atanasov et al., 2021). The rich regime is often defined purely in distinction to the lazy regime; however, recent work has refined this dichotomy by demonstrating that both the relative and absolute scale of initial weights across layers induce a continuum of feature-learning dynamics and corresponding inductive

biases (Woodworth et al., 2020; Azulay et al., 2021; Domínguez et al., 2024; Kunin et al., 2024). Our work builds on these insights to show how this spectrum manifests in the PT+FT setting. We show that, depending on task parameters, intermediate regimes can induce superior generalization, suggesting that analyses restricted to extreme cases may miss important behaviors.

Implicit Regularization and Diagonal Linear Networks.

Neural networks are often trained in an overparameterized setting where there are many possible solutions to the training data. In this setting, the training procedure consistently biases the network towards a particular solution (a phenomenon called “implicit bias”, Soudry et al., 2018), explaining why neural networks generalize well even without explicit regularization (Zhang et al., 2016). Lazy and rich regimes often instantiate fundamentally distinct implicit biases. Lazy-regime neural networks implement a kernel predictor, whereas rich-regime neural networks are often biased towards learning low-dimensional or sparse representations (Gunasekar et al., 2018; Savarese et al., 2019; Lyu & Li, 2019; Nacson et al., 2019; Chizat & Bach, 2020). Diagonal linear networks (Section 3.1) instantiate a simple, analytically tractable model that captures the changes in inductive bias observed in more complex models: lazy-regime training finds the (non-sparse) solution with minimal ℓ_2 -norm, whereas rich-regime training finds the sparse solution with minimal ℓ_1 -norm (Woodworth et al., 2020; Azulay et al., 2021). Prior work has characterized the emergence of the infinite-time solution in these networks (Pesme & Flammarion, 2023; Berthier, 2023) and investigated the role of stochasticity and step size (Pesme et al., 2021; Nacson et al., 2022).

Implicit Regularization of Fine-Tuning. In dense linear networks, a higher similarity in task features between pretraining and fine-tuning generally improves generalization performance (Lampinen & Ganguli, 2018; Shachaf et al., 2021; Tahir et al., 2024). Moreover, fine-tuning with backpropagation can result in improved in-distribution generalization compared to only training the linear readout, but may harm out-of-distribution performance (Kumar et al., 2022; Tomihari & Sato, 2024). These theories generally focus on single-output dense linear networks (which have the same inductive bias in the rich and lazy regime) or training in the kernel regime (Malladi et al., 2023). In contrast, our perspective allows us to characterize how different pretraining initializations shift the fine-tuning behavior between the lazy and rich regime. Other works characterize the influence of pretraining data selection on fine-tuning under distributional shifts (Kang et al., 2024; Cohen-Wang et al., 2024; Jain et al., 2025). Finally, Lippl & Lindsey (2024) characterized the inductive bias of

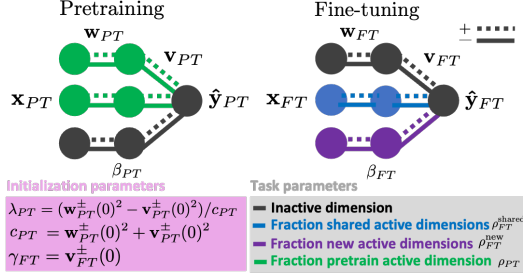


Figure 1. **Setup.** Schematic illustration of the theoretical setup: dependence on the initialization parameters c_{PT} , λ_{PT} , and γ_{FT} (shown in pink); and dependence on the data parameters ρ_{PT} , $\rho_{FT}^{\text{shared}}$, and ρ_{FT}^{new} (shown in grey).

diagonal linear networks for infinitesimal initial weights in pretraining and studied the resulting generalization behavior using simulations in a teacher-student setup. Here we substantially extend their work by characterizing the inductive bias conferred by a broad range of pretraining and fine-tuning initializations, revealing a crucial role played by the relative scale of initialization. Moreover, we derive an analytical theory describing the generalization error (rather than relying on simulations), providing closer insight into specific conditions under which certain pretraining initializations help or hurt performance.

Replica-theoretical Characterization of the Generalization Error. We leverage the replica method (Edwards & Anderson, 1975; Mézard et al., 1987) to characterize the ability of diagonal linear networks to recover ground-truth parameters in a fine-tuning setup. The replica method is non-rigorous, but provides a powerful tool for analytically characterizing estimation errors in the high-dimensional limit under different penalties, including ℓ_1 (Guo & Verdú, 2005; Rangan et al., 2009). These formulas were later confirmed using rigorous approaches (Bayati & Montanari, 2011a;b). We specifically rely on the approach in Boreyhi & Müller (2018); Boreyhi et al. (2019), which characterizes estimation errors with potentially different penalties across dimensions. Our results imply that pretraining can be understood as modifying the penalties across different dimensions; this is related to prior work on incorporating prior knowledge on the support in compressed sensing problems (Khajehnejad et al., 2009; Vaswani & Lu, 2010).

3. Theoretical Setup

3.1. Network Architecture

We study the generalization behavior of *diagonal linear networks* (Fig. 1), a simple one-hidden-layer network archi-

tecture that parametrizes linear maps $f : \mathbb{R}^D \rightarrow \mathbb{R}$ as

$$f_{\mathbf{w}, \mathbf{v}}(\mathbf{x}) = \beta(\mathbf{w}, \mathbf{v})^T \mathbf{x}, \quad (1)$$

where $\beta(\mathbf{w}, \mathbf{v}) := \mathbf{v}^+ \circ \mathbf{w}^+ - \mathbf{v}^- \circ \mathbf{w}^- \in \mathbb{R}^D$ (\circ indicates element-wise multiplication). Here, \mathbf{w}^+ , $\mathbf{w}^- \in \mathbb{R}^D$ comprise the hidden weights of the network and \mathbf{v}^+ , $\mathbf{v}^- \in \mathbb{R}^D$ comprise its output weights. \mathbf{w}^+ , \mathbf{v}^+ and \mathbf{w}^- , \mathbf{v}^- parameterize the positive and negative pathway, respectively; separating these pathways allows us to initialize the network at $\beta = 0$ while avoiding a saddle point.

Diagonal linear networks capture two key aspects of the deep neural networks used in practice: 1) their initial weights control their transition between the rich (feature-learning) and lazy (kernel) regime and 2) their generalization behavior is different between these regimes (Woodworth et al., 2020; Azulay et al., 2021; Lippl & Lindsey, 2024). They therefore provide a useful theoretical model to study the impact of initialization on pretraining and fine-tuning.

3.2. Network Training

We investigate diagonal linear networks trained with gradient flow to minimize mean-squared error. We consider two datasets: a pretraining (PT) task $\mathbf{X}_{PT} \in \mathbb{R}^{N_{PT} \times D}$, $\mathbf{y}_{PT} \in \mathbb{R}^{N_{PT}}$ and a fine-tuning (FT) task $\mathbf{X}_{FT} \in \mathbb{R}^{N_{FT} \times D}$, $\mathbf{y}_{FT} \in \mathbb{R}^{N_{FT}}$. The training proceeds in two stages: we first pretrain on the PT task and then fine-tune on the FT task (PT+FT). In both cases, we assume that the model trains to zero training error. We denote the parameters learned during pretraining and fine-tuning by $\mathbf{w}_{PT}(t)$, $\mathbf{v}_{PT}(t)$ and $\mathbf{w}_{FT}(t)$, $\mathbf{v}_{FT}(t)$, the corresponding network functions by $\hat{\beta}_{PT}(t)$ and $\hat{\beta}_{FT}(t)$, and their predictions by $\hat{\mathbf{y}}_{PT} = \mathbf{X}_{PT} \hat{\beta}_{PT}$ and $\hat{\mathbf{y}}_{FT} = \mathbf{X}_{FT} \hat{\beta}_{FT}$. t denotes the learning time, $t = 0$ indicating the initial weights, and $t = \infty$ the weights at the end of training. Where the context is clear, we denote the network functions at the end of pretraining and fine-tuning by $\hat{\beta}_{PT}$ and $\hat{\beta}_{FT}$.

Initialization. We assume $w^+(0) = w^-(0)$ and $v^+(0) = v^-(0)$ (to avoid biasing the network towards positive or negative coefficients). Building on insights from the feature learning literature, we focus on two key aspects of the weight initialization: 1) the **absolute scale** (capturing the overall initial weight magnitude),

$$c_{PT} := \mathbf{w}_{PT}^\pm(0)^2 + \mathbf{v}_{PT}^\pm(0)^2, \quad (2)$$

and 2) the **relative scale** (capturing the difference in initial weight magnitude between the first and the second layer),

$$\lambda_{PT} := (\mathbf{w}_{PT}^\pm(0)^2 - \mathbf{v}_{PT}^\pm(0)^2)/c_{PT} \in [-1, 1]. \quad (3)$$

After pretraining, we re-balance the positive and negative pathways by setting

$$\mathbf{w}_{FT}^\pm(0) := \mathbf{w}_{PT}^+(\infty) + \mathbf{w}_{PT}^-(\infty), \quad (4)$$

to ensure that the effective network function at the beginning of fine-tuning is zero again: $\beta_{FT}(0) = 0$. Further, we re-initialize the readout weights to a fixed scale $\gamma_{FT} \geq 0$:

$$\mathbf{v}_{FT}^\pm(0) := \gamma_{FT}. \quad (5)$$

By systematically varying these three initialization parameters (c_{PT} , λ_{PT} , and γ_{FT}), we aim to understand their effect on fine-tuning performance.

3.3. Data Generative Model

To investigate the generalization performance of diagonal linear networks trained in this manner, we consider a *teacher-student setup*, where we sample ground-truth pretraining and fine-tuning functions (“teachers”) by sampling from a joint distribution $\beta_{PT}^*, \beta_{FT}^* \sim p_{PT,FT}(\beta_{PT}^*, \beta_{FT}^*)$. We generate the dataset by sampling random inputs, $\mathbf{X}_{PT}, \mathbf{X}_{FT} \sim \mathcal{N}(0, \frac{1}{D})$, and generating the outputs through the teachers, $\mathbf{y}_{PT} = \mathbf{X}_{PT}\beta_{PT}^*$, $\mathbf{y}_{FT} = \mathbf{X}_{FT}\beta_{FT}^*$. We aim to characterize the deviation between the ground-truth β_{FT}^* and the estimate resulting from fine-tuning, $\hat{\beta}_{FT}$:

$$\mathcal{E} := \|\beta_{FT}^* - \hat{\beta}_{FT}\|_2^2. \quad (6)$$

We characterize \mathcal{E} through a replica-theoretical approach, which describes the network behavior in the high-dimensional limit ($D \rightarrow \infty$), where we scale the pretraining and fine-tuning data size with D :

$$\alpha_{PT} := \lim_{D \rightarrow \infty} N_{PT}/D, \quad \alpha_{FT} := \lim_{D \rightarrow \infty} N_{FT}/D. \quad (7)$$

We will focus on the case $\alpha_{PT} \geq 1$, and as a result $\hat{\beta}_{PT} = \beta_{PT}^*$ is perfectly recovered. We call α_{FT} (also known as the “load”) the *data scale*. Finally, we characterize a specific family of generative models $p_{PT,FT}(\beta_{PT}^*, \beta_{FT}^*)$, in which there are J underlying groups that are sampled with probabilities $\pi \in \mathbb{R}^J$ for each dimension $d \in \{1, \dots, D\}$. For the sampled group $j \in \{1, \dots, J\}$, $\beta_{PT,d}^*$ and $\beta_{FT,d}^*$ are independently sampled from group-specific distributions $p_{PT}^{(j)}$ and $p_{FT}^{(j)}$, i.e. their dependency is mediated via their group membership (see Definition C.1).

To investigate the consequences of our theory (and confirm it in empirical simulations), we will focus on a **spike-and-slab** distribution for $\beta_{PT}^*, \beta_{FT}^*$. In diagonal linear networks, feature learning is useful when only a sparse subset of dimensions are active for a given task. We therefore sample the set of active dimensions for the pretraining task,

$$\theta_{PT} \sim \text{Bernoulli}(\rho_{PT}), \quad \theta_{PT} \in \{0, 1\}^D, \quad (8)$$

and then generate β_{PT} by sampling random signs for the active dimensions (i.e. any d for which $\theta_d = 1$):

$$\beta_{PT} = (\sigma/\sqrt{\rho_{PT}}) \circ \theta_{PT}, \quad \sigma \sim \text{Cat}(\{-1, 1\}). \quad (9)$$

We similarly assume that a subset of dimensions is active on the fine-tuning task by sampling $\theta_{FT} \in \{0, 1\}^D$. However, in this case, whether a given dimension is active can depend on whether it was already active on the pretraining task:

$$\begin{aligned} \theta_{FT} | \theta_{PT} = 1 &\sim \text{Bernoulli}(\rho_{FT}^{\text{shared}}/\rho_{PT}), \\ \theta_{FT} | \theta_{PT} = 0 &\sim \text{Bernoulli}(\rho_{FT}^{\text{new}}/(1 - \rho_{PT})), \\ \beta_{FT} &= b_{FT} \circ \theta_{FT}, \quad b_{FT} \sim \mathcal{N}(0, \frac{1}{\rho_{FT}^{\text{shared}} + \rho_{FT}^{\text{new}}}). \end{aligned} \quad (10)$$

Thus, $\rho_{FT}^{\text{shared}} \geq \rho_{FT}^{\text{new}}$ means that dimensions active during pretraining are more likely to be active during fine-tuning, whereas $\rho_{FT}^{\text{shared}} \leq \rho_{FT}^{\text{new}}$ means that they are less likely. **Fig. 1** depicts the network configuration varying the task parameters.

Taken together, we will characterize how 1) initialization parameters, c_{PT} , λ_{PT} , and γ_{FT} , 2) task parameters, ρ_{PT} , $\rho_{FT}^{\text{shared}}$, and ρ_{FT}^{new} , and 3) data scale, α_{FT} , impact generalization during fine-tuning.

4. Theoretical Characterization of Generalization Error in Fine-Tuning

We will derive a theoretical characterization of the generalization error \mathcal{E} in two steps: first, we will derive the implicit regularization induced by PT+FT in diagonal linear networks as a function of initialization parameters (Theorem 4.1), then we will characterize the generalization error induced by the different possible regularization penalties for our data generative model (Proposition 4.2).

4.1. Implicit Inductive Bias of Fine-Tuning

We first derive the implicit inductive bias of overparameterized diagonal networks under the fine-tuning training paradigm, building on analysis in prior work (Azulay et al., 2021; Lippl & Lindsey, 2024).

Theorem 4.1 (Implicit bias). *Consider a diagonal linear network trained under the paradigm described in Section 3.2. Then, the gradient flow solution at convergence is*

given by

$$\arg \min_{\beta_{FT}} Q_k(\beta_{FT}) \quad \text{s.t. } \mathbf{X}_{FT}^\top \beta_{FT} = \mathbf{y}_{FT}, \quad (11)$$

$$\text{where } Q_k(\beta_{FT}) = \sum_{d=1}^D q_{k_d}(\beta_{FT,d}), \quad (12)$$

$$q_k(z) = \frac{\sqrt{k}}{4} \left(1 - \sqrt{1 + \frac{4z^2}{k}} + \frac{2z}{\sqrt{k}} \operatorname{arcsinh} \left(\frac{2z}{\sqrt{k}} \right) \right), \quad (13)$$

$$k_d = \left(2c_{PT}(1 + \lambda_{PT}) \left(1 + \sqrt{1 + (\hat{\beta}_{PT,d}/c_{PT})^2} \right) + \gamma^2 \right)^2. \quad (14)$$

Proof. Azulay et al. (2021) proved that c_{PT} (when defined as $c_{PT} = w^+ w^- + v^+ v^-$) and λ_{PT} are conserved throughout training (see also Marcotte et al., 2023). Extended calculations allow us to recover the individual layers’ weights from the effective network weights after pretraining. Details are relegated to Appendix B.1 due to space constraints. \square

Theorem 4.1 shows that the function selected by the network depends on λ_{PT} , c_{PT} , and γ_{FT} in a non-trivial manner. Importantly, this implicit bias also depends on $\hat{\beta}_{PT}$, implying that the learned solution potentially depends on the pretraining task. Notably, even though in diagonal linear networks, the relative scale λ_{PT} does not impact the inductive bias of pretraining, it does impact the learned hidden representation and therefore the inductive bias of fine-tuning. In Section 5.1 we show how these dependencies shape the resulting learning regime. This substantially extends results by Lippl & Lindsey (2024), which focused on $c_{PT} \rightarrow 0$ with $\lambda_{PT} = 0, \gamma_{FT} = 0$. We will show that this only captures a subset of the range of learning regimes we identify. In particular, and perhaps surprisingly, we will see that even for very small c_{PT} , different values for λ_{PT} can fundamentally change the generalization behavior.

4.2. Replica Theory of the Generalization Error

In practice, this implicit bias manifests in the sample efficiency and generalization performance observed during fine-tuning. To understand the impact of the implicit bias derived in Theorem 4.1 on generalization, we now turn to solving the corresponding optimization problem.

$$\hat{\beta} := \arg \min_{\beta \in \mathbb{R}^D} \frac{1}{2\lambda} \|\mathbf{X}_{FT}\beta - \mathbf{y}_{FT}\|_2^2 + Q_k(\beta_{FT}), \quad (15)$$

$$\beta \in \mathbb{R}^D, k \in \mathbb{R}_+^D.$$

For $\lambda \rightarrow 0$, this precisely characterizes the implicit inductive bias of a diagonal linear network trained on the training data $(\mathbf{X}_{FT}, \mathbf{y}_{FT})$. We aim to characterize how accurately

this optimization problem can recover the ground-truth vector $\beta_{FT}^* \in \mathbb{R}^D$, given the label

$$\mathbf{y}_{FT} = \mathbf{X}_{FT}\beta_{FT}^* + \varepsilon, \quad \varepsilon \sim \mathcal{N}(0, \sigma_0^2). \quad (16)$$

Note that while our theory also applies to $\sigma_0^2 > 0$, we will focus on the noiseless case $\sigma_0^2 = 0$. We assume that $\beta_{FT}^*, \beta_{PT}^*$ are sampled from the joint distribution described above. This connects our setting to the setting studied in Beryhi & Müller (2018), allowing us to characterize the generalization error in the high-dimensional limit.

Proposition 4.2. *Let $N_{FT} \rightarrow \infty$ and $N_{FT}/D \rightarrow \alpha_{FT} > 0$. Then, under the replica assumption, the estimation problem (15) decouples into a scalar problem*

$$\hat{\beta}^{sc}(y; k, \theta) := \arg \min_{\beta \in \mathbb{R}} \left\{ \frac{(y - \beta)^2}{2\theta} + Q_k(\beta) \right\}. \quad (17)$$

Specifically, $(\beta_d^*, \hat{\beta}_d, k_d)$ converge in distribution to

$$\hat{\beta}_d = \hat{\beta}^{sc}(\beta_d^* + \eta; k_d, \theta), \quad \eta \sim \mathcal{N}(0, \theta_0). \quad (18)$$

Here θ and θ_0 are the “effective” regularization and noise parameters. They are not only governed by the external noise and regularization, but also by the noise and regularization induced from estimating the other parameters. These two properties are governed by the fixed-point equations

$$p = \sum_{j=1}^J \pi_j \mathbb{E}_{\beta^*, k, \eta} \left[(\hat{\beta}^{sc}(\beta^* + \eta; k, \theta) - \beta^*)^2 \right], \quad (19)$$

$$\chi = \theta \sum_{j=1}^J \pi_j \mathbb{E}_{\beta^*, k, \eta} \left[\partial_y \hat{\beta}^{sc}(\beta^* + \eta; k, \theta) \right], \quad (20)$$

$$\text{where } \theta = \frac{\lambda + \chi}{\alpha}, \quad \theta_0 = \frac{\sigma_0^2 + p}{\alpha}.$$

Proof. The proposition follows from Proposition 1 in Beryhi & Müller (2018), see Appendix C. \square

This proposition, paired with Theorem 4.1, yields an exact formula for the generalization error associated with PT+FT in diagonal linear networks, as a function of weight initialization, task parameters, and data scale.

5. Understanding Learning Regimes in PT+FT

The theoretical insights developed in Section 4 help us understand the inductive bias of PT+FT across the full spectrum of weight initialization and task parameters. We first use Theorem 4.1 to characterize how the initialization parameters influence the network’s learning regime (Sections 5.1 and 5.2) and then use Proposition 4.2 to tie these different learning regimes to the task parameters for which they are favorable (Section 5.3).

5.1. Learning Regimes in the Limit

Building on Theorem 4.1, we characterize the learning regime of the networks using two measures (introduced in Lippl & Lindsey (2024)):

1. The ℓ -order $:= \frac{\partial \log q_{k_d}(\beta_{FT,d})}{\partial \log |\beta_{FT,d}|}$, measures whether the network benefits from sparsity. ℓ -order = 1 indicates a sparse inductive bias (e.g. the ℓ_1 -norm), whereas ℓ -order = 2 corresponds to a non-sparse inductive bias (e.g. the ℓ_2 -norm).
2. The pretraining dependence¹, $PD := \frac{\partial \log q_{k_d}(\beta_{PT,d})}{\partial \log |\beta_{PT,d}|}$ measures whether the network benefits from pretrained features. $PD = -1$ indicates that the penalty is inversely proportional to the magnitude of the pretrained feature $|\beta_{PT,d}|$, whereas $PD = 0$ indicates that the penalty does not depend on it at all. While the ℓ -order arises as a relevant quantity in single-task learning as well, PD only arises in a multi-task setting.

We derive analytical formulas for these metrics as a function of both the initialization parameters and $\beta_{PT,d}$ and $\beta_{FT,d}$ (see Appendix B.2). We further identify a universal tension between ℓ -order and PD :

Proposition 5.1. *We identify the following ranges across the full spectrum of initialization: ℓ -order $\in [1, 2]$, $PD \in [-1, 0]$, ℓ -order + $PD \in [1, 2]$.*

Proof. We derive these ranges in Appendix B.2. They extend a finding from Lippl & Lindsey (2024) who found that ℓ -order + $PD = 1$ for $c_{PT} \rightarrow 0$, $\lambda_{PT}, \gamma_{FT} = 0$. \square

In Fig. 2a, we identify three limiting regimes arising from the interplay between the ℓ -order and pretraining dependence. Taking appropriate limits of the initialization parameters λ_{PT} and c_{PT} places the model in these regimes, each corresponding to familiar norm-based regularization:

- (I) A **rich, pretraining-independent regime**, (new dimensions learned; ℓ -order = 1, $PD = 0$). This regime is governed by the ℓ_1 -norm: $Q(\beta_{FT}) \rightarrow \|\beta_{FT}\|_1$ and is induced, for instance, in the limit $\lambda_{PT} \rightarrow -1$, $\gamma_{FT} \rightarrow 0$. We call an ℓ_1 -like inductive bias in diagonal linear networks “rich”, because it arises from the feature-learning dynamics (see Section 2).
- (II) A **lazy, pretraining-dependent regime**, (reuse with minimal adaptation; ℓ -order = 2, $PD = -1$). This regime is governed by the weighted ℓ_2 -norm: $Q(\beta_{FT}) \rightarrow$

¹Lippl & Lindsey (2024) introduced this metric as feature dependence; we call it pretraining dependence to emphasize that it characterizes the dependence on the pretraining function directly.

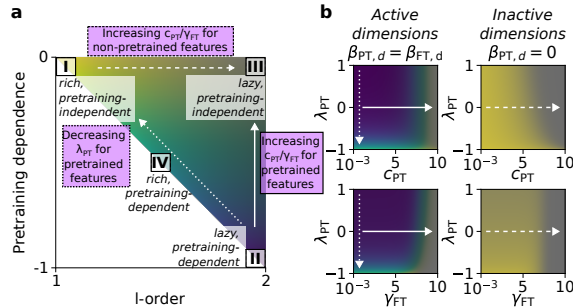


Figure 2. **Implicit bias and learning regimes of fine-tuning.** (a) ℓ -order and pretraining dependence jointly define four different learning regimes in PT+FT. Different initialization parameters induce changes between these learning regimes, as indicated by the arrows. (b) We can interpolate between these four regimes (for a color legend, see panel (a)) by shifting the initialization parameters ($\hat{\beta}_{FT,d} = 1/\sqrt{\rho_{FT}}$, $\rho_{FT} = 0.1$). Crucial transitions, which we further highlight in the text and in panel (a), are indicated by the arrows. Simulation details can be found in Appendix E.

$\sum_{i=1}^D |\beta_{FT,i}|^2 / |\beta_{PT,i}|$. This regime is induced, for instance, by considering $c_{PT} \rightarrow 0$ and $\lambda_{PT} \rightarrow 1$.

- (III) A **lazy, pretraining-independent regime** (ℓ -order = 2, $PD = 0$). This regime is governed by the unweighted ℓ_2 -norm: $Q(\beta_{FT}) \rightarrow \|\beta_{FT}\|_2$ and implies that the fine-tuning behavior does not depend on the pretraining task at all. This regime is induced, for instance, by taking $c_{PT} \rightarrow \infty$ or $\gamma_{FT} \rightarrow \infty$.

We highlight the identification of a novel regime—the *lazy, pretraining-independent regime*—which goes beyond previous works. This regime is accessible only in the fine-tuning setting and highlights that for badly chosen initialization parameters, pretraining will not create transferable features.

5.2. Full Phase Portrait of the Learning Regimes

In Section 5.1, our analysis was restricted to asymptotic behavior. However, in practice we may be operating in an intermediate learning regime where the parameters do not approach one of the above limits. Indeed, operating in such a regime will often confer a beneficial inductive bias: On the one hand, for pretraining to be useful, the penalty should depend on the active pretraining dimensions, i.e. ideally $PD = -1$. On the other hand, a sparse inductive bias substantially improves generalization performance (if the ground truth is also sparse), i.e. ideally ℓ -order = 1. Proposition 5.1 highlights a fundamental tradeoff between these desiderata: it is impossible to achieve $PD = -1$ and ℓ -order = 1. The set of possible values for the pair (ℓ -order, PD) is given by a triangle whose edges are given by regimes (I-III) (Fig. 2b). We thus highlight an important intermediate regime:

- (IV) The **pretraining-dependent rich regime** (ℓ -order <

2, $PD < 0$) achieves a balance between pretraining dependence and ℓ -order, enabling the model to leverage both sparsity and feature reuse simultaneously.

Overall, the four learning regimes we highlight are distinguished by their pretraining dependence and sparsity bias/ ℓ -order. To understand how the initialization parameters impact the learning regime, we plot the full phase portrait of the learning regimes as a function of pretraining initialization (**Fig. 2b**), considering a typical value at the end of training, $\beta_{FT,d} = 1/\sqrt{\rho_{FT}}$ (setting $\rho_{FT} = 0.1$ as this will be a common task setting in the subsequent section). We note that because of our task generation process, we either have $\beta_{PT,d}^* = \pm 1/\sqrt{\rho_{PT}}$ (setting $\rho_{PT} = 0.1$ as well) or $\beta_{PT,d}^* = 0$. We therefore plot the phase diagram for both cases, which clarifies which learning regime we operate in for active dimensions ($\beta_{PT,d}^* = \pm 1/\sqrt{\rho_{PT}}$) and inactive dimensions ($\beta_{PT,d}^* = 0$).

For active dimensions where $\beta_{PT,d}^* = \pm 1/\sqrt{\rho_{PT}}$, changing the relative scale λ_{PT} shifts the network from the *lazy, pretraining-dependent regime* (II) to the *rich, pretraining-independent regime* (I), with intermediate scales yielding the *rich, pretraining-dependent regime* (IV) (see the dotted line in **Fig. 2a,b**). Intuitively, a negative λ_{PT} implies that the second-layer weights dominate over the first layer ($v > w$), while a positive λ_{PT} indicates the opposite ($w > v$). When λ_{PT} is large and negative, the first-layer representation is comparatively small, even after pretraining. After rescaling the second layer to $\gamma_{FT} = 0$, these large second-layer weights are reduced, decreasing the overall scale of the network—this drives the system toward the rich regime. In contrast, as λ_{PT} increases, the learned first-layer representation becomes larger, driving the network into the *lazy, pretraining-dependent regime*. In contrast, increasing the absolute scale c_{PT} or the fine-tuning re-initialization scale γ_{FT} moves the system toward the *lazy pretraining-independent regime* (III), where neither sparsity nor shared dimensions improve generalization (solid line in **Fig. 2a,b**).

For inactive dimensions ($\beta_{PT,d}^* = 0$), we find that $PD = 0$. Thus, instead of the two-dimensional continuum outlined above, we recover a one-dimensional continuum between the *lazy pretraining-independent regime* (III) and the *rich pretraining-independent regime* (I) (**Fig. 2b**, right column). Increasing γ_{FT} or c_{PT} shifts the inductive bias from regime (I) into regime (III) (see the dashed line in **Fig. 2a,b**). Additionally, (albeit less pronounced), increasing λ_{PT} also shifts the inductive bias into a slightly lazier regime.

Overall, the different initialization parameters can therefore

change the inductive bias of PT+FT along three axes: they can control 1) whether the network benefits from shared dimensions with the pretraining task (measured by the PD for active dimensions), 2) whether the network benefits from sparsity in the new active dimensions (measured by the ℓ -order for $\beta_{PT,d}^* = 0$), and 3) whether the network benefits from sparsity in the shared active dimensions (measured by the ℓ -order for active dimensions). In the next section, we leverage Proposition 4.2 to show that this allows us to understand how these different initializations impact generalization performance across task parameters.

5.3. Learning Regime and Task Parameters Jointly Determine Generalization Error Curves

In practice, the implicit bias described above is reflected in the sample efficiency and generalization performance observed during fine-tuning. We solve the fixed-point equations derived in Proposition 4.2 to understand how the different learning regimes and task parameters impact generalization performance. In particular, we examine the impact of the different initialization parameters on the three axes outlined above. We additionally directly train diagonal linear networks in a PT+FT setup to validate our analytical characterization with empirical simulations.

Do we benefit from shared dimensions? If our penalty implements pretraining dependence, we should benefit from sharing dimensions between pretraining and fine-tuning. We therefore consider a fixed $\rho_{PT} = 0.1$ and compare the case $\rho_{FT}^{\text{shared}} = 0.1, \rho_{FT}^{\text{new}} = 0$ (in which case the pretraining and fine-tuning task share all their dimensions) to the case $\rho_{FT}^{\text{shared}} = 0, \rho_{FT}^{\text{new}} = 0.1$ (in which case they share no dimensions, but the overall sparsity level is matched). As c_{PT} and γ_{FT} decrease, performance becomes increasingly sensitive to task overlap (**Fig. 3a,b**). On the other hand, decreasing λ_{PT} decreases the extent to which we benefit from shared dimensions (**Fig. 3c**). These trends are consistent with the phase-portrait analysis, which indicates that for pretrained dimensions, decreasing γ_{FT} and c_{PT} at fixed λ_{PT} shifts the network from a *lazy, pretraining-independent regime* toward a *lazy, pretraining-dependent regime* (solid line in **Fig. 2**). In contrast, decreasing λ_{PT} shifts the model from a *lazy, pretraining-dependent regime* to a *rich, pretraining-independent regime* (dotted line in **Fig. 2**).

Do we benefit from sparsity in new active dimensions?

For inactive dimensions (i.e. $\beta_{PT,d}^* = 0$), we can either be in a rich regime where we benefit from a sparse set of new dimensions, or a lazy regime where we learn sparse and non-sparse sets equally well. We therefore consider a task with no shared dimensions with the pretraining task ($\rho_{PT} = 0.1, \rho_{FT}^{\text{shared}} = 0$) and compare performance across different levels of sparsity on the

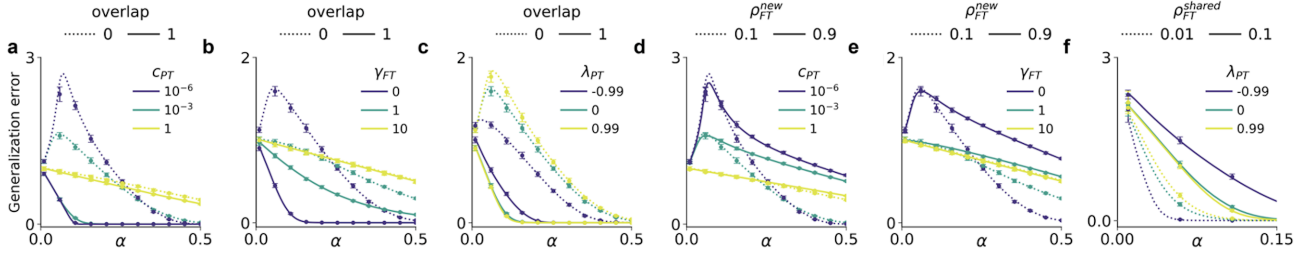


Figure 3. Generalization curves for different initialization parameters and task parameters. The generalization error \mathcal{E} as a function of the data scale α_{FT} . Lines depict replica predictions and points depict the results of our empirical simulations (± 2 standard errors). In all cases, $\rho_{PT} = 0.1$. We consider $c_{PT} = 10^{-3}$, $\lambda_{PT} = 0$, and $\gamma_{FT} = 0$, varying one initialization parameter for each panel. Simulation details can be found in Appendix E. (a-c) We consider either overlapping ($\rho_{FT}^{\text{shared}} = 0.1$, $\rho_{FT}^{\text{new}} = 0$) or distinct ($\rho_{FT}^{\text{shared}} = 0$, $\rho_{FT}^{\text{new}} = 0.1$) FT dimensions. (d,e) We consider $\rho_{FT}^{\text{shared}} = 0$ and vary ρ_{FT}^{new} . (f) We consider $\rho_{FT}^{\text{shared}} = 0$ and vary ρ_{FT}^{new} .

fine-tuning task ($\rho_{FT} = 0.1, 0.9$). We observe that as c_{PT} and γ_{FT} decrease, sparsity becomes increasingly beneficial for performance (**Fig. 3d,e**). This observation aligns with the phase-portrait analysis, which shows that for $\beta_{PT,d}^* = 0$ the model undergoes a transition from a *lazy, pretraining-independent regime*, which has no sparsity bias, to a *rich, pretraining-independent regime* that supports the learning of new, useful dimensions and has a sparsity bias (dashed line in **Fig. 2**).

Do we benefit from sparsity in shared active dimensions?

Rich learning regimes should also benefit from sparsity in pretrained dimensions (with $\beta_{PT,d}^* = \pm 1/\sqrt{\rho_{PT}}$). We therefore consider fully overlapping dimensions ($\rho_{PT} = 0.1$, $\rho_{FT}^{\text{new}} = 0$) and compare $\rho_{FT}^{\text{shared}} = 0.1$ to $\rho_{FT}^{\text{shared}} = 0.01$. We observe that as λ_{PT} decreases, the network increasingly benefits from sparsity (**Fig. 3f**). However, this effect vanishes if c_{PT} or γ_{FT} are very large. This observation again aligns with the phase-portrait analysis: as λ_{PT} decreases, we move into the *rich, pretraining-dependent regime* (dotted line in **Fig. 2**), but if c_{PT} or γ_{FT} increase, we move into the *lazy, pretraining-independent regime* regardless of λ_{PT} .

Taken together, the generalization curves elucidate how initialization parameters interact with task parameters to shape generalization behavior. In particular, the generalization curves demonstrate the same trade-off between sparsity and pretraining dependence we predicted from Proposition 5.1: as λ_{PT} becomes more negative, we move along the diagonal representing the trade-off between ℓ -order and pretraining dependence (dotted line in **Fig. 2**). As a result, the network benefits less from overlap: for $\rho_{FT}^{\text{shared}} = 0.1$ (indicating a full overlap between pretrained and fine-tuned dimensions), decreasing λ_{PT} makes generalization worse (**Fig. 3f**). At the same time, the network benefits more from sparsity: for $\rho_{FT}^{\text{shared}} = 0.01$, trading off a stronger sparsity bias for a weaker pretraining dependence is worthwhile, and a smaller

λ_{PT} yields better performance. Overall, this identifies λ_{PT} as a crucial factor for changing the inductive bias of PT+FT and highlights that the optimal learning regime will depend on the task parameters (see **Fig. 5** in the Appendix).

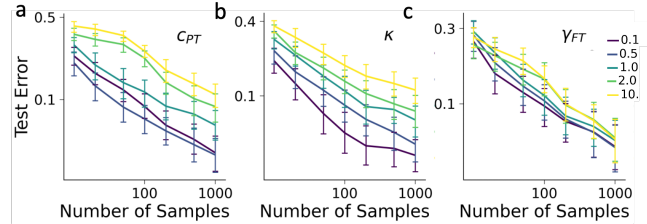


Figure 4. ResNet CIFAR-100. Generalization performance as a function of the number of samples and initialization parameters. We vary (a) the absolute scale of initialization by multiplying all weights in the network by c_{PT} , (b) the relative scale of initialization by multiplying the first three blocks of the ResNet by κ (equivalent to λ_{PT}), and (c) the readout initialization by multiplying the readout by γ_{FT} (Simulation details: Appendix E).

6. Large-Scale Vision Experiments

Our theoretical analysis and small-scale experiments suggest that modifying pretraining parameters and rescaling parameters provides a theoretically principled mechanism for inducing useful feature learning during fine-tuning. To evaluate this prediction, we pretrain a ResNet on 98 classes from CIFAR-100 and subsequently fine-tune it on the remaining two classes. The class split is sampled randomly and repeated fifty times. We design three experimental settings that translate the theoretical parameters λ_{PT} , c_{PT} , and γ_{FT} to a realistic deep-network architecture. The ResNet-18 architecture consists of an initial embedding layer followed by four stages of residual blocks, each containing two convolutional layers with identity skip connections. To induce imbalance across network layers, we upscale the embedding layer and the first three residual stages by a constant factor κ . To implement an equivalent notion of c_{PT} scaling in this architecture, we scale all

network parameters by a constant factor. Finally, to implement an analogue of γ_{FT} , we rescale the parameters of the final classification layer after pretraining² Further experimental details are provided in Appendix D.

In **Fig. 4a**, we observe that a ResNet initialized with a non-standard small value of κ —where $\kappa < 1$ corresponds to a negative relative scaling—exhibits improved generalization during fine-tuning. Similarly, as shown in **Fig. 4b**, increasing the scale of c_{PT} also leads to degraded fine-tuning generalization, in agreement with our theoretical predictions. Finally, **Fig. 4c** shows that decreasing the scale of γ_{FT} improves fine-tuning generalization for intermediate sample sizes. In Appendix D, we provide a representation-level analysis of the three settings, finding that all three settings induce a key representational signature indicative of the *pretraining-dependent rich regime*. All parameters identified by the theory have a meaningful impact on generalization during fine-tuning in practice. However, these results should be interpreted with caution when extrapolating to large-scale architectures, as several key differences, including depth and nonlinearities, may affect their applicability (discussed in Appendix D).

7. Conclusion

Despite the prevalence of the pretraining–fine-tuning (PT+FT) pipeline in modern deep learning, a comprehensive understanding of the inductive bias of PT+FT, and how it relates to initialization structure and task parameters, has remained elusive. Here we developed an end-to-end theory of PT+FT in diagonal linear networks, analytically computing the generalization error as a function of initialization parameters, task parameters, and data scale. Albeit based on a simplified neural network model, our analysis provides quantitative insights relevant to practical scenarios in machine learning and neuroscience. In particular, it underscores the importance of relative weight scales across layers. Extending this framework to nonlinear networks represents an important next step. Finally, measuring the ℓ -order and pretraining dependence in more complex architectures—e.g. using influence functions (Koh & Liang, 2017)—could help uncover how feature reuse and adaptation arise during learning across both artificial and biological systems.

Impact Statement

This paper presents work whose goal is to advance the field of Machine Learning. There are many potential societal consequences of our work, none of which we feel must be specifically highlighted here.

²For completeness, we report in Appendix D the heuristic proposed by Lippl & Lindsey (2024).

Acknowledgements

NA thanks the Rafael del Pino Foundation for financial support. This research was funded in whole or in part by the Austrian Science Fund (FWF) 10.55776/COE12. SL acknowledges support by NSF 1707398 (Neuronex) and Gatsby Charitable Foundation GAT3708. This work was supported by a Schmidt Science Polymath Award to AS, and the Sainsbury Wellcome Centre Core Grant from Wellcome (219627/Z/19/Z) and the Gatsby Charitable Foundation (GAT3850). FM is funded by a MRC Career Development Award (MR/T010614/1), a UKRI Advanced Pain Discovery Platform grant (MR/W027593/1), and a EPSRC/MRC Programme Grant (UKRI1970). For the purpose of open access, the authors have applied a CC BY public copyright license to any Author Accepted Manuscript version arising from this submission.

References

- Atanasov, A., Bordelon, B., and Pehlevan, C. Neural networks as kernel learners: The silent alignment effect, 10 2021. URL <https://openreview.net/forum?id=1NvflqAdoom>.
- Awais, M., Naseer, M., Khan, S., Anwer, R. M., Cholakkal, H., Shah, M., Yang, M.-H., and Khan, F. S. Foundation models defining a new era in vision: a survey and outlook. *IEEE Transactions on Pattern Analysis and Machine Intelligence*, 2025.
- Azulay, S., Moroshko, E., Nacson, M. S., Woodworth, B. E., Srebro, N., Globerson, A., and Soudry, D. On the implicit bias of initialization shape: Beyond infinitesimal mirror descent. In *International Conference on Machine Learning*, pp. 468–477. PMLR, 2021.
- Bayati, M. and Montanari, A. The dynamics of message passing on dense graphs, with applications to compressed sensing. *IEEE Transactions on Information Theory*, 57(2):764–785, 2011a.
- Bayati, M. and Montanari, A. The lasso risk for gaussian matrices. *IEEE Transactions on Information Theory*, 58(4):1997–2017, 2011b.
- Bereyhi, A. and Müller, R. R. Maximum-a-posteriori signal recovery with prior information: Applications to compressive sensing. In *2018 IEEE International Conference on Acoustics, Speech and Signal Processing (ICASSP)*, pp. 4494–4498. IEEE, 2018.
- Bereyhi, A., Müller, R. R., and Schulz-Baldes, H. Statistical mechanics of map estimation: General replica ansatz. *IEEE Transactions on Information Theory*, 65(12):7896–7934, 2019.

- Berthier, R. Incremental learning in diagonal linear networks. *Journal of Machine Learning Research*, 24(171): 1–26, 2023.
- Bommasani, R. On the opportunities and risks of foundation models. *arXiv preprint arXiv:2108.07258*, 2021.
- Braun, L., Dominé, C., Fitzgerald, J., and Saxe, A. Exact learning dynamics of deep linear networks with prior knowledge. *Advances in Neural Information Processing Systems*, 35:6615–6629, 12 2022.
- Chizat, L. and Bach, F. Implicit bias of gradient descent for wide two-layer neural networks trained with the logistic loss. In *Conference on learning theory*, pp. 1305–1338. PMLR, 2020.
- Chizat, L., Oyallon, E., and Bach, F. On lazy training in differentiable programming. *Advances in neural information processing systems*, 32, 2019.
- Cohen-Wang, B., Vendrow, J., and Madry, A. Ask your distribution shift if pre-training is right for you. *arXiv preprint arXiv:2403.00194*, 2024.
- Dominé, C. C., Anguita, N., Proca, A. M., Braun, L., Kunin, D., Mediano, P. A., and Saxe, A. M. From lazy to rich: Exact learning dynamics in deep linear networks. *arXiv preprint arXiv:2409.14623*, 2024.
- Edwards, S. F. and Anderson, P. W. Theory of spin glasses. *Journal of Physics F: Metal Physics*, 5(5):965, 1975.
- Fort, S., Dziugaite, G. K., Paul, M., Kharaghani, S., Roy, D. M., and Ganguli, S. Deep learning versus kernel learning: an empirical study of loss landscape geometry and the time evolution of the neural tangent kernel. *Advances in Neural Information Processing Systems*, 33: 5850–5861, 2020.
- Gao, P., Trautmann, E., Yu, B., Santhanam, G., Ryu, S., Shenoy, K., and Ganguli, S. A theory of multineuronal dimensionality, dynamics and measurement. *BioRxiv*, pp. 214262, 2017.
- Giaffar, H., Buxó, C. R., and Aoi, M. The effective number of shared dimensions between paired datasets. In *International Conference on Artificial Intelligence and Statistics*, pp. 4249–4257. PMLR, 2024.
- Gunasekar, S., Lee, J., Soudry, D., and Srebro, N. Characterizing implicit bias in terms of optimization geometry. In *International Conference on Machine Learning*, pp. 1832–1841. PMLR, 2018.
- Guo, D. and Verdú, S. Randomly spread cdma: Asymptotics via statistical physics. *IEEE Transactions on Information Theory*, 51(6):1983–2010, 2005.
- Huh, M., Agrawal, P., and Efros, A. A. What makes imagenet good for transfer learning? *arXiv preprint arXiv:1608.08614*, 2016.
- Jacot, A., Gabriel, F., and Hongler, C. Neural tangent kernel: Convergence and generalization in neural networks. *Advances in neural information processing systems*, 31, 2018.
- Jain, A., Montanari, A., and Sasoglu, E. Train on Validation (ToV): Fast data selection with applications to fine-tuning. *arXiv preprint arXiv:2510.00386*, 2025.
- Jain, S., Kirk, R., Lubana, E. S., Dick, R. P., Tanaka, H., Grefenstette, E., Rocktäschel, T., and Krueger, D. S. Mechanistically analyzing the effects of fine-tuning on procedurally defined tasks. *arXiv preprint arXiv:2311.12786*, 2023.
- Kang, F., Just, H. A., Sun, Y., Jahagirdar, H., Zhang, Y., Du, R., Sahu, A. K., and Jia, R. Get more for less: Principled data selection for warming up fine-tuning in llms. *arXiv preprint arXiv:2405.02774*, 2024.
- Khajehnejad, M. A., Xu, W., Avestimehr, A. S., and Hassibi, B. Weighted ℓ_1 minimization for sparse recovery with prior information. In *2009 IEEE international symposium on information theory*, pp. 483–487. IEEE, 2009.
- Koh, P. W. and Liang, P. Understanding black-box predictions via influence functions. In *International conference on machine learning*, pp. 1885–1894. PMLR, 2017.
- Kumar, A., Raghunathan, A., Jones, R., Ma, T., and Liang, P. Fine-tuning can distort pretrained features and underperform out-of-distribution. *arXiv preprint arXiv:2202.10054*, 2022.
- Kunin, D., Raventós, A., Dominé, C., Chen, F., Klindt, D., Saxe, A., and Ganguli, S. Get rich quick: exact solutions reveal how unbalanced initializations promote rapid feature learning, 06 2024. URL <https://arxiv.org/abs/2406.06158>.
- Lampinen, A. K. and Ganguli, S. An analytic theory of generalization dynamics and transfer learning in deep linear networks. *arXiv preprint arXiv:1809.10374*, 2018.
- Lippl, S. and Lindsey, J. Inductive biases of multi-task learning and finetuning: multiple regimes of feature reuse. In *The Thirty-eighth Annual Conference on Neural Information Processing Systems*, 2024.
- Lyu, K. and Li, J. Gradient descent maximizes the margin of homogeneous neural networks. *arXiv preprint arXiv:1906.05890*, 2019.

- Malladi, S., Wettig, A., Yu, D., Chen, D., and Arora, S. A kernel-based view of language model fine-tuning. In *International Conference on Machine Learning*, pp. 23610–23641. PMLR, 2023.
- Marcotte, S., Gribonval, R., and Peyré, G. Abide by the law and follow the flow: conservation laws for gradient flows, 12 2023. URL https://proceedings.neurips.cc/paper_files/paper/2023/hash/c7bee9b76be21146fd592fc2b46614d5-Abstract-Conference.html.
- Mézard, M., Parisi, G., and Virasoro, M. A. *Spin glass theory and beyond: An Introduction to the Replica Method and Its Applications*, volume 9. World Scientific Publishing Company, 1987.
- Müller, R. R., Alfano, G., Zaidel, B. M., and de Miguel, R. Applications of large random matrices in communications engineering. *arXiv preprint arXiv:1310.5479*, 2013.
- Nacson, M. S., Gunasekar, S., Lee, J., Srebro, N., and Soudry, D. Lexicographic and depth-sensitive margins in homogeneous and non-homogeneous deep models. In *International Conference on Machine Learning*, pp. 4683–4692. PMLR, 2019.
- Nacson, M. S., Ravichandran, K., Srebro, N., and Soudry, D. Implicit bias of the step size in linear diagonal neural networks. In *International Conference on Machine Learning*, pp. 16270–16295. PMLR, 2022.
- Parthasarathy, V. B., Zafar, A., Khan, A., and Shahid, A. The ultimate guide to fine-tuning llms from basics to breakthroughs: An exhaustive review of technologies, research, best practices, applied research challenges and opportunities. *arXiv preprint arXiv:2408.13296*, 2024.
- Pesme, S. and Flammarion, N. Saddle-to-saddle dynamics in diagonal linear networks. *Advances in Neural Information Processing Systems*, 36:7475–7505, 2023.
- Pesme, S., Pillaud-Vivien, L., and Flammarion, N. Implicit bias of sgd for diagonal linear networks: a provable benefit of stochasticity. *Advances in Neural Information Processing Systems*, 34:29218–29230, 2021.
- Rangan, S., Goyal, V., and Fletcher, A. K. Asymptotic analysis of map estimation via the replica method and compressed sensing. *Advances in Neural Information Processing Systems*, 22, 2009.
- Savarese, P., Evron, I., Soudry, D., and Srebro, N. How do infinite width bounded norm networks look in function space? In *Conference on Learning Theory*, pp. 2667–2690. PMLR, 2019.
- Saxe, A., McClelland, J. L., and Ganguli, S. Exact solutions to the nonlinear dynamics of learning in deep linear neural networks. *openreview.net*, 12 2013. URL https://openreview.net/forum?id=_wzZwKpTDF_9C.
- Saxe, A. M., McClelland, J. L., and Ganguli, S. A mathematical theory of semantic development in deep neural networks. *Proceedings of the National Academy of Sciences*, 116(23):11537–11546, 2019.
- Shachaf, G., Brutzkus, A., and Globerson, A. A theoretical analysis of fine-tuning with linear teachers. *Advances in Neural Information Processing Systems*, 34:15382–15394, 2021.
- Soudry, D., Hoffer, E., Nacson, M. S., Gunasekar, S., and Srebro, N. The implicit bias of gradient descent on separable data. *Journal of Machine Learning Research*, 19 (70):1–57, 2018.
- Tahir, J., Ganguli, S., and Rotskoff, G. M. Features are fate: a theory of transfer learning in high-dimensional regression. *arXiv preprint arXiv:2410.08194*, 2024.
- Tomihari, A. and Sato, I. Understanding linear probing then fine-tuning language models from ntk perspective. *Advances in Neural Information Processing Systems*, 37: 139786–139822, 2024.
- Vaswani, N. and Lu, W. Modified-cs: Modifying compressive sensing for problems with partially known support. *IEEE Transactions on Signal Processing*, 58(9):4595–4607, 2010. doi: 10.1109/TSP.2010.2051150.
- Vyas, N., Bansal, Y., and Nakkiran, P. Limitations of the ntk for understanding generalization in deep learning. *arXiv preprint arXiv:2206.10012*, 2022.
- Woodworth, B., Gunasekar, S., Lee, J. D., Moroshko, E., Savarese, P., Golan, I., Soudry, D., and Srebro, N. Kernel and rich regimes in overparametrized models. In *Conference on Learning Theory*, pp. 3635–3673. PMLR, 2020.
- Yosinski, J., Clune, J., Bengio, Y., and Lipson, H. How transferable are features in deep neural networks? *Advances in neural information processing systems*, 27, 2014.
- Zhang, C., Bengio, S., Hardt, M., Recht, B., and Vinyals, O. Understanding deep learning requires rethinking generalization. *arXiv preprint arXiv:1611.03530*, 2016.

A. Extended Results

We showcase the four limit regimes by plotting the generalization curves across three different ground truth structures, varying sparsity and overlap:

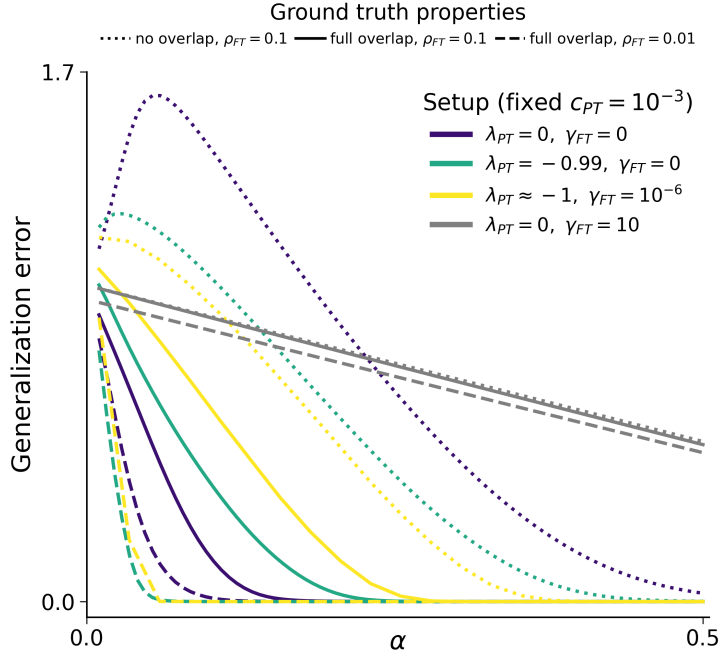


Figure 5. Comparison of the four fine-tuning learning regimes. We show three task parameter settings: 1) no overlap between pretraining and fine-tuning dimensions; 2) identical pretraining and fine-tuning dimensions; 3) fine-tuning dimension as a subset of pretraining dimensions. We show for different initialization parameter settings: a lazy, pretraining-dependent regime (II, shown in purple), a lazy, pretraining-independent regime (III, shown in grey), an intermediate rich, pretraining-dependent regime (IV, shown in green), and a richer, less pretraining-dependent regime (I, shown in yellow). We observe that for the task parameter setting without any overlap, the regime approaching the rich, pretraining-independent regime (in yellow) is optimal. For the complete overlap between pretraining and fine-tuning dimensions, the lazy, pretraining-dependent regime (II, in purple) is optimal. Finally, for the task where the fine-tuning dimensions are a subset of pretraining dimensions, the rich, pretraining-dependent regime (IV, in green) is optimal. All of these observations are predicted by our theoretical insight in the inductive bias of PT+FT.

B. Theoretical Analysis of the PT+FT Learning Regimes

B.1. Implicit Bias

Theorem 4.1 (Implicit bias). *Consider a diagonal linear network trained under the paradigm described in Section 3.2. Then, the gradient flow solution at convergence is given by*

$$\arg \min_{\beta_{FT}} Q_k(\beta_{FT}) \quad \text{s.t. } \mathbf{X}_{FT}^\top \beta_{FT} = \mathbf{y}_{FT}, \quad (11)$$

$$\text{where } Q_k(\beta_{FT}) = \sum_{d=1}^D q_{k_d}(\beta_{FT,d}), \quad (12)$$

$$q_k(z) = \frac{\sqrt{k}}{4} \left(1 - \sqrt{1 + \frac{4z^2}{k}} + \frac{2z}{\sqrt{k}} \operatorname{arcsinh} \left(\frac{2z}{\sqrt{k}} \right) \right), \quad (13)$$

$$k_d = \left(2c_{PT}(1 + \lambda_{PT}) \left(1 + \sqrt{1 + (\hat{\beta}_{PT,d}/c_{PT})^2} \right) + \gamma^2 \right)^2. \quad (14)$$

Proof. We follow a similar proof method as in (Azulay et al., 2021). We assume the pretraining quantities:

$$\begin{aligned}\mathbf{w}^+(0)^2 - \mathbf{v}^+(0)^2 &= \tilde{\lambda}_{PT} \\ \mathbf{w}^-(0)^2 - \mathbf{v}^-(0)^2 &= \tilde{\lambda}_{PT} \\ \mathbf{w}^+(0)\mathbf{w}^-(0) + \mathbf{v}^+(0)\mathbf{v}^-(0) &= c_{PT},\end{aligned}$$

where $\lambda_{PT} = \tilde{\lambda}_{PT}/c_{PT}$.

We reparameterize as :

$$\begin{aligned}\mathbf{w}^+ &= \sqrt{\tilde{\lambda}_{PT}} \cosh \theta^+, & \mathbf{w}^- &= \sqrt{\tilde{\lambda}_{PT}} \cosh \theta^- \\ \mathbf{v}^+ &= \sqrt{\tilde{\lambda}_{PT}} \sinh \theta^+, & \mathbf{v}^- &= \sqrt{\tilde{\lambda}_{PT}} \sinh \theta^-.\end{aligned}$$

We use the conserved quantities $c_{PT}, \tilde{\lambda}_{PT}$ to get an expression for θ^+ and θ^- :

$$\begin{aligned}\cosh \theta^+ \cosh \theta^- + \sinh \theta^+ \sinh \theta^- &= \frac{c_{PT}}{\tilde{\lambda}_{PT}} \\ \cosh \theta^+ \sinh \theta^+ - \cosh \theta^- \sinh \theta^- &= \frac{\beta_{PT}}{\tilde{\lambda}_{PT}}\end{aligned}$$

Therefore, we have

$$\begin{aligned}\mathbf{w}^+ &= \sqrt{\tilde{\lambda}_{PT}} \cosh \left(\frac{1}{2} \left[\operatorname{arcosh} \left(\frac{c_{PT}}{\tilde{\lambda}_{PT}} \right) + \operatorname{arsinh} \left(\frac{\beta_{PT}}{c_{PT}} \right) \right] \right) \\ \mathbf{v}^+ &= \sqrt{\tilde{\lambda}_{PT}} \sinh \left(\frac{1}{2} \left[\operatorname{arcosh} \left(\frac{c_{PT}}{\tilde{\lambda}_{PT}} \right) + \operatorname{arsinh} \left(\frac{\beta_{PT}}{c_{PT}} \right) \right] \right) \\ \mathbf{w}^- &= \sqrt{\tilde{\lambda}_{PT}} \cosh \left(\frac{1}{2} \left[\operatorname{arcosh} \left(\frac{c_{PT}}{\tilde{\lambda}_{PT}} \right) - \operatorname{arsinh} \left(\frac{\beta_{PT}}{c_{PT}} \right) \right] \right) \\ \mathbf{v}^- &= \sqrt{\tilde{\lambda}_{PT}} \sinh \left(\frac{1}{2} \left[\operatorname{arcosh} \left(\frac{c_{PT}}{\tilde{\lambda}_{PT}} \right) - \operatorname{arsinh} \left(\frac{\beta_{PT}}{c_{PT}} \right) \right] \right)\end{aligned}$$

After pretraining, we reinitialize parameters:

$$\begin{aligned}\mathbf{w}_{FT}^+(0) &= \mathbf{w}_{FT}^-(0) = \mathbf{w}_{PT}^+(\infty) + \mathbf{w}_{PT}^-(\infty) \\ \mathbf{v}_{FT}^+(0) &= \mathbf{v}_{FT}^-(0) = \gamma_{FT}.\end{aligned}$$

We are interested in the initial conserved quantity before finetuning, c_{FT} .

By definition, we have

$$\begin{aligned}c_{FT} &= \mathbf{w}_{FT}^+(0)\mathbf{w}_{FT}^-(0) + \mathbf{v}_{FT}^+(0)\mathbf{v}_{FT}^-(0) \\ &= (\mathbf{w}_{PT}^+(\infty) + \mathbf{w}_{PT}^-(\infty))^2 + \gamma_{FT}^2 \\ &= (\mathbf{w}_{PT}^+(\infty))^2 + 2\mathbf{w}_{PT}^+(\infty)\mathbf{w}_{PT}^-(\infty) + (\mathbf{w}_{PT}^-(\infty))^2 + \gamma_{FT}^2.\end{aligned}$$

Let

$$A = \operatorname{arcosh} \left(\frac{c_{PT}}{\tilde{\lambda}_{PT}} \right), \quad B = \operatorname{arsinh} \left(\frac{\beta_{PT}}{c_{PT}} \right).$$

We compute:

$$\begin{aligned}\mathbf{w}_{PT}^+(\infty)^2 &= \tilde{\lambda}_{PT} \cosh^2\left(\frac{1}{2}(A+B)\right) = \tilde{\lambda}_{PT} \left(\frac{1 + \cosh(A+B)}{2}\right) \\ \mathbf{w}_{PT}^-(\infty)^2 &= \tilde{\lambda}_{PT} \cosh^2\left(\frac{1}{2}(A-B)\right) = \tilde{\lambda}_{PT} \left(\frac{1 + \cosh(A-B)}{2}\right)\end{aligned}$$

Thus, we have

$$\mathbf{w}_{PT}^+(\infty)^2 + \mathbf{w}_{PT}^-(\infty)^2 = \tilde{\lambda}_{PT} \left(1 + \frac{\cosh(A+B) + \cosh(A-B)}{2}\right).$$

Recall the identity:

$$\cosh(A+B) + \cosh(A-B) = 2 \cosh A \cosh B.$$

Therefore, we have

$$\mathbf{w}_{PT}^+(\infty)^2 + \mathbf{w}_{PT}^-(\infty)^2 = \tilde{\lambda}_{PT} (1 + \cosh A \cosh B).$$

Now,

$$\begin{aligned}2\mathbf{w}_{PT}^+(\infty)\mathbf{w}_{PT}^-(\infty) &= 2\sqrt{\tilde{\lambda}_{PT}} \cosh\left(\frac{A+B}{2}\right) \cdot \sqrt{\tilde{\lambda}_{PT}} \cosh\left(\frac{A-B}{2}\right) \\ &= 2\tilde{\lambda}_{PT} \cosh\left(\frac{A+B}{2}\right) \cosh\left(\frac{A-B}{2}\right) \\ &= \tilde{\lambda}_{PT} (\cosh A + \cosh B),\end{aligned}$$

using the identity $2 \cosh x \cosh y = \cosh(x+y) + \cosh(x-y)$.

Let us compute:

$$\cosh A = \frac{c_{PT}}{\tilde{\lambda}_{PT}}, \quad \cosh B = \cosh\left(\operatorname{asinh}\left(\frac{\beta_{aux}}{c_{PT}}\right)\right) = \sqrt{1 + \left(\frac{\beta_{aux}}{c_{PT}}\right)^2},$$

$$\begin{aligned}c_{FT} &= \tilde{\lambda}_{PT} \frac{c_{PT}}{\tilde{\lambda}_{PT}} \sqrt{1 + \left(\frac{\beta_{PT}}{c_{PT}}\right)^2} \\ &\quad + \tilde{\lambda}_{PT} \left(\frac{c_{PT}}{\tilde{\lambda}_{PT}} + \sqrt{1 + \left(\frac{\beta_{PT}}{c_{PT}}\right)^2}\right) + \gamma_{FT}^2 \\ c_{FT} &= (\tilde{\lambda}_{PT} + c_{PT}) \left(1 + \sqrt{1 + \left(\frac{\beta_{PT}}{c_{PT}}\right)^2}\right) + \gamma_{FT}^2.\end{aligned}$$

Now, from [Azulay et al. \(2021\)](#), we know that the implicit bias of a diagonal linear network is parameterized as in Eq. (1) that converges to a zero loss solution can be expressed as:

$$\beta_*(\infty) = \arg \min_{\beta_{FT}} Q_k(\beta_{FT}) \quad \text{s.t.} \quad \mathbf{X}_{FT}^\top \beta_{FT} = \mathbf{y}_{FT},$$

$$\text{where} \quad Q_k(\beta_{FT}) = \sum_{i=1}^D q_{k_i}(\beta_{FT,i}),$$

$$\text{with } q_k(z) = \frac{\sqrt{k}}{4} \left(1 - \sqrt{1 + \frac{4z^2}{k}} + \frac{2z}{\sqrt{k}} \operatorname{arcsinh} \left(\frac{2z}{\sqrt{k}} \right) \right),$$

where $k_i = 4c_i^2$. In our case $k_i = 4c_{FT,i}^2 = \left(2(\tilde{\lambda}_{PT,i} + c_{PT,i}) \left(1 + \sqrt{1 + (\beta_{PT,i}/c_{PT,i})^2} \right) + \gamma_{FT}^2 \right)^2$. Hence $k_i = 4c_{FT,i}^2$. The theorem follows from replacing $\tilde{\lambda}_{PT,i} = \lambda_{PT,i} c_{PT,i}$. \square

B.2. Pretraining Importance and ℓ -order

We now derive an analytical expression for ℓ -order and pretraining dependence (PD), where

$$\ell\text{-order} := \frac{\partial \log q_k(\beta_{FT})}{\partial \log \beta_{FT}} \quad \text{and} \quad PD := \frac{\partial \log q_k(\beta_{FT})}{\partial \log \beta_{PT}}. \quad (21)$$

We define

$$\zeta := \frac{2\beta_{FT}}{\sqrt{k}}, \quad s := \frac{\beta_{PT}}{c_{PT}}, \quad \phi(z) = 1 - \sqrt{1 + z^2} + z \operatorname{arcsinh}(z). \quad (22)$$

We additionally define the quantity

$$\kappa := \frac{\partial \log k}{\partial \log \beta_{PT}}. \quad (23)$$

Intuitively, κ captures how much a certain function that was learned during pretraining transfers to fine-tuning features.

Proposition B.1. *We find that*

$$\ell\text{-order} = \frac{\zeta \operatorname{asinh}(\zeta)}{\phi(\zeta)}, \quad (24)$$

$$PD = \frac{1 - \ell\text{-order}}{2} \kappa. \quad (25)$$

where

$$\kappa = \frac{4c_{PT}(1 + \lambda_{PT})s^2}{(2c_{PT}(1 + \lambda_{PT})(1 + \sqrt{1 + s^2}) + \gamma_{FT}^2)\sqrt{1 + s^2}}. \quad (26)$$

Notably,

$$\ell\text{-order} \in [1, 2], \quad \kappa \in [0, 2], \quad PD \in [-1, 0], \quad (27)$$

and

$$\ell\text{-order} + PD \in [1, 2] \quad (28)$$

Proof. First, with $\zeta := 2\beta_{FT}/\sqrt{k}$ we can rewrite

$$q_k(\beta_{FT}) = \frac{\sqrt{k}}{4} \left(1 - \sqrt{1 + \zeta^2} + \zeta \operatorname{arcsinh}(\zeta) \right) = \frac{\sqrt{k}}{4} \phi(\zeta).$$

We now first derive the closed forms before deriving bounds for the different quantities.

Closed form for ℓ -order. For fixed k ,

$$\ell\text{-order} = \frac{\partial \log q_k(\beta_{FT})}{\partial \log \beta_{FT}} = \frac{\partial \log \phi(\zeta)}{\partial \log \zeta} = \zeta \frac{\phi'(\zeta)}{\phi(\zeta)}.$$

Since $\phi'(\zeta) = \operatorname{asinh}(\zeta)$,

$$\ell\text{-order} = \frac{\zeta \operatorname{asinh}(\zeta)}{\phi(\zeta)}.$$

Closed form for κ . Write $\sqrt{k} = A$ where

$$A := 2(\hat{\lambda}_{PT} + c_{PT})(1 + \sqrt{1 + s^2}) + \gamma_{FT}^2, \quad s := \beta_{PT}/c_{PT}.$$

Then $k = A^2$, so

$$\kappa = \frac{\partial \log k}{\partial \log \beta_{PT}} = 2 \frac{\partial \log A}{\partial \log \beta_{PT}}.$$

Since $s = \beta_{PT}/c_{PT}$ we have $\partial \log s / \partial \log \beta_{PT} = 1$. Also,

$$\frac{d}{ds} \sqrt{1 + s^2} = \frac{s}{\sqrt{1 + s^2}}, \quad \Rightarrow \quad \frac{\partial A}{\partial s} = 2(\hat{\lambda}_{PT} + c_{PT}) \frac{s}{\sqrt{1 + s^2}}.$$

Thus

$$\frac{\partial \log A}{\partial \log \beta_{PT}} = \frac{s}{A} \frac{\partial A}{\partial s} = \frac{s}{A} \cdot 2(\hat{\lambda}_{PT} + c_{PT}) \frac{s}{\sqrt{1 + s^2}} = \frac{2(\hat{\lambda}_{PT} + c_{PT})s^2}{A\sqrt{1 + s^2}},$$

and therefore

$$\kappa = \frac{4(\hat{\lambda}_{PT} + c_{PT})s^2}{A\sqrt{1 + s^2}} = \frac{4(\hat{\lambda}_{PT} + c_{PT})s^2}{(2(\hat{\lambda}_{PT} + c_{PT})(1 + \sqrt{1 + s^2}) + \gamma_{FT}^2)\sqrt{1 + s^2}}.$$

Closed form for PD . By definition,

$$PD = \frac{\partial \log q_k(\beta_{FT})}{\partial \log \beta_{PT}} = \frac{\partial \log q_k(\beta_{FT})}{\partial \log k} \cdot \frac{\partial \log k}{\partial \log \beta_{PT}} = \frac{\partial \log q_k(\beta_{FT})}{\partial \log k} \cdot \kappa.$$

Now

$$\log q_k(\beta_{FT}) = \frac{1}{2} \log k + \log \phi(\zeta) - \log 4,$$

and $\frac{\partial \log \zeta}{\partial \log k} = -1/2$. Hence

$$\frac{\partial \log q_k(\beta_{FT})}{\partial \log k} = \frac{1}{2} + \frac{\partial \log \phi(\zeta)}{\partial \log \zeta} \cdot \frac{\partial \log \zeta}{\partial \log k} = \frac{1}{2} - \frac{1}{2} \ell\text{-order},$$

which yields

$$PD = \left(\frac{1}{2} - \frac{1}{2} \ell\text{-order} \right) \kappa = \frac{1 - \ell\text{-order}}{2} \kappa.$$

Bounding ℓ -order. Assume $\zeta \geq 0$. First, since $1 - \sqrt{1 + \zeta^2} \leq 0$,

$$\phi(\zeta) \leq \zeta \operatorname{arcsinh}(\zeta) \quad \Rightarrow \quad \ell\text{-order} = \frac{\zeta \operatorname{arcsinh}(\zeta)}{\phi(\zeta)} \geq 1.$$

For the upper bound, we show $\phi(\zeta) \geq \frac{1}{2}\zeta \operatorname{arcsinh}(\zeta)$, i.e.

$$\zeta \operatorname{arcsinh}(\zeta) \geq 2(\sqrt{1 + \zeta^2} - 1).$$

Let $\zeta = \sinh t$ with $t = \operatorname{arcsinh}(\zeta) \geq 0$, so $\sqrt{1 + \zeta^2} = \cosh t$. The inequality becomes

$$t \sinh t \geq 2(\cosh t - 1).$$

Define $h(t) := t \sinh t - 2(\cosh t - 1)$. Then $h(0) = 0$,

$$h'(t) = t \cosh t - \sinh t, \quad h''(t) = t \sinh t \geq 0 \quad (t \geq 0).$$

Thus h' is increasing and $h'(0) = 0$, so $h'(t) \geq 0$ for $t \geq 0$, implying $h(t) \geq 0$. Hence $\ell\text{-order} \leq 2$.

Bounding κ . Clearly $\kappa \geq 0$. Also $A \geq 2(\hat{\lambda}_{PT} + c_{PT})(1 + \sqrt{1 + s^2})$, so

$$\kappa \leq \frac{4(\hat{\lambda}_{PT} + c_{PT})s^2}{2(\hat{\lambda}_{PT} + c_{PT})(1 + \sqrt{1 + s^2})\sqrt{1 + s^2}} = 2 \cdot \frac{s^2}{\sqrt{1 + s^2}(1 + \sqrt{1 + s^2})}.$$

Let $B := \sqrt{1 + s^2} \geq 1$. Since $s^2 = B^2 - 1$,

$$2 \cdot \frac{B^2 - 1}{B(1 + B)} = 2 \cdot \frac{B - 1}{B} < 2,$$

with equality approached only in the limit $B \rightarrow \infty$ and $\gamma_{FT} \rightarrow 0$. Hence $\kappa \in [0, 2)$.

Bounding PD and ℓ -order+ PD . From $PD = \frac{1 - \ell\text{-order}}{2}\kappa$, the bounds $\ell\text{-order} \in [1, 2]$ and $\kappa \in [0, 2)$ imply

$$PD \leq 0, \quad PD \geq \frac{1 - 2}{2} \cdot 2 = -1,$$

so $PD \in [-1, 0]$. Finally,

$$\ell\text{-order} + PD = \ell\text{-order} + \frac{1 - \ell\text{-order}}{2}\kappa = \left(1 - \frac{\kappa}{2}\right)\ell\text{-order} + \frac{\kappa}{2}.$$

Since $\kappa/2 \in [0, 1)$, this is a convex combination of $\ell\text{-order} \in [1, 2]$ and 1, hence it lies in $[1, 2]$. \square

C. Replica Theory

C.1. Proof of Proposition 4.2

We consider the following generative model for $(\beta_{PT,d}^*, \beta_{FT,d})$.

Definition C.1. We assume that there are J underlying groups. Each group is sampled with probability π_j , $\sum_{j=1}^J \pi_j = 1$, denoted by $j \sim \text{Cat}(\pi)$. Each group has associated pretraining and fine-tuning distributions $p_{PT}^{(j)}$ and $p_{FT}^{(j)}$ which are independent when conditioned on j :

$$j \sim \text{Cat}(\pi), \quad \beta_{PT,d}^* \sim p_{PT}^{(j)}, \quad \beta_{FT,d}^* \sim p_{FT}^{(j)}. \quad (29)$$

This means that any dependence between β_{PT} and β_{FT} is mediated by their respective group membership j . We apply Proposition 1 of [Bereyhi & Müller \(2018\)](#) to the estimator (15).

Step 1: Notation. We begin by noting a few notational differences to their setting. Specifically, to translate our setting into theirs, we set

$$A := X, \quad x := \beta, \quad c_d := k_d, \quad u_j(v; c) := q_c(v). \quad (30)$$

Moreover,

$$g_j^{\text{dec}} \equiv \hat{\beta}^{\text{sc}}, \quad (31)$$

except that we write out the dependence on θ explicitly. Finally, they treat (c_d) as a deterministic sequence, whereas we consider a particular probability distribution for each block, $p_c^{(j)}$. However, because they average over coordinates, we know that this converges to the corresponding block-mixture expectations, weighted by $\pi_j = \lim_{D \rightarrow \infty} |B_j|/D$.

Step 2: Simplifying for i.i.d. X_{FT} . Proposition 1 of [Bereyhi & Müller \(2018\)](#) states that in the high-dimensional limit, the joint law of a typical coordinate decouples into a scalar Gaussian channel: for $d \in B_j$,

$$(\beta_d^*, \hat{\beta}_d, k_d) \Rightarrow (\beta^*, \hat{\beta}^{\text{sc}}(\beta^* + \eta; k, \theta), k), \quad \eta \sim \mathcal{N}(0, \theta_0),$$

where $(\beta^*, k) \sim p_\beta^{(j)} \otimes p_k^{(j)}$ and the block is drawn according to π_j . Moreover, the scalar estimator is the MAP operator

$$\hat{\beta}^{\text{sc}}(y; k, \theta) := \arg \min_{\beta \in \mathbb{R}} \left\{ \frac{(y - \beta)^2}{2\theta} + Q_k(\beta) \right\},$$

which matches our definition. Notably, this result depends on a few assumptions (detailed in [Bereyhi & Müller \(2018\)](#) and [Bereyhi et al. \(2019\)](#)): we assume that the parameters describing β_j become deterministic in the high-dimensional limit, that we can exchange the limit between the moment m and the data size n and, most crucially, that we can analytically continue the computed moments for discrete m to the real domain so as to take the limit $m \rightarrow 0$.

Step 3: Simplifying the fixed-point equations. We now consider their resulting fixed-point equations and show how they evaluate to the fixed-point equations presented in our proposition. First, we note that because X is i.i.d. with variance $1/D$, we can evaluate the R-transform. As, X has variance $1/D$, $\frac{1}{\alpha}X$ has variance $1/N$. Thus, $R_{\frac{1}{\alpha}X}(\omega) = \frac{\alpha}{\alpha - \omega}$. By the properties of the R-transform (see e.g. [Müller et al. \(2013\)](#)),

$$R_X(\omega) = \alpha R_{\frac{1}{\alpha}X}(\alpha\omega) = \frac{\alpha}{1 - \omega}. \quad (32)$$

Thus,

$$\theta = \frac{\lambda + \chi}{\alpha}, \quad \theta_0 = \frac{\sigma_0^2 + p}{\alpha}. \quad (33)$$

For the fixed-point equation for χ , we additionally simplify the expression a little bit:

$$\begin{aligned} \frac{\theta_0}{\theta} \chi &= \sum_{j=1}^J \pi_j \mathbb{E}_{\beta^*, k, \eta} \left[(\hat{\beta}^{\text{sc}}(\beta^* + \eta; k, \theta) - \beta^*) \eta \right] \stackrel{(1)}{=} \sum_{j=1}^J \pi_j \mathbb{E}_{\beta^*, k, \eta} \left[\hat{\beta}^{\text{sc}}(\beta^* + \eta; k, \theta) \eta \right] \\ &\stackrel{(2)}{=} \theta_0 \sum_{j=1}^J \pi_j \mathbb{E}_{\beta^*, k, \eta} \left[\partial_y \hat{\beta}^{\text{sc}}(\beta^* + \eta; k, \theta) \right], \end{aligned} \quad (34)$$

where (1) arises from the fact that β^* and η are independent and $\mathbb{E}[\eta] = 0$ and (2) is a direct application of Stein's lemma,

$$\mathbb{E}[X f(X)] = \sigma^2 \mathbb{E}[f'(X)] \text{ for } X \sim \mathcal{N}(0, \sigma^2). \quad (35)$$

Hence, we can reduce the original matrix-valued fixed point equations to a system of scalar fixed-point equations in the parameters (p, χ) .

Expressing $\partial_y \hat{\beta}(y; k, \theta)$. Denoting

$$q'_k(x) := \frac{\partial q_k(x)}{\partial x}, \quad q''_k(x) := \frac{\partial^2 q_k(x)}{\partial x^2}, \quad (36)$$

the first-order optimality condition for

$$\hat{\beta}^{\text{sc}}(y; k, \theta) = \arg \min_{\beta} \frac{(y - \beta)^2}{2\theta} + q_k(\beta)$$

is

$$0 = \frac{1}{\theta} (\hat{\beta}^{\text{sc}}(y; k, \theta) - y) + q'_k(\hat{\beta}^{\text{sc}}(y; k, \theta)).$$

Implicit differentiation with respect to y gives

$$\partial_y \hat{\beta}^{\text{sc}}(y; k, \theta) = \frac{1}{1 + \theta q''_k(\hat{\beta}^{\text{sc}}(y; k, \theta))}.$$

We note that

$$q'_k(z) = \frac{1}{2} \operatorname{asinh} \left(\frac{2z}{\sqrt{k}} \right), \quad q''_k(z) = \frac{1}{\sqrt{k + 4z^2}}. \quad (37)$$

Substituting $\beta = \hat{\beta}^{\text{sc}}(y; k, \theta)$ yields the explicit Jacobian

$$\partial_y \hat{\beta}^{\text{sc}}(y; k, \theta) = \frac{1}{1 + \frac{\theta}{\sqrt{k + 4\hat{\beta}^{\text{sc}}(y; k, \theta)^2}}},$$

$$p = \sum_{j=1}^J \pi_j \mathbb{E}_{\beta^*, k, \eta} [(\hat{\beta}^{\text{sc}}(\beta^* + \eta; k, \theta) - \beta^*)^2], \quad (38)$$

$$\chi = \theta_0 \sum_{j=1}^J \pi_j \mathbb{E}_{\beta^*, \eta} \left[\left(1 + \frac{\theta}{\sqrt{k + 4\hat{\beta}^{\text{sc}}(\beta^* + \eta; k, \theta)^2}} \right)^{-1} \right], \quad (39)$$

with the closure relations

$$\theta = \frac{\lambda + \chi}{\alpha}, \quad \theta_0 = \frac{\sigma_0^2 + p}{\alpha}. \quad (40)$$

This proves the proposition.

D. Large-Scale Vision Experiments

In this section, we provide a more detailed description of the experiments conducted on ResNet architectures in different settings. We pair the accuracy results presented with a measure of the representation before and after fine-tuning. We employ the commonly used *participation ratio* (PR; (Gao et al., 2017)) as a measure of dimensionality, and the *effective number of shared dimensions* (ENSD; (Giaffar et al., 2024)) as a measure of the number of principal components aligned between two representations. Intuitively, the PR and ENSD of network representations before and after fine-tuning capture the key phenomenology of the pretraining-dependent rich regime.

Specifically, we expect that the dimensionality of the network representation X_{FT} after fine-tuning is lower than that of the representation X_{PT} after pretraining, i.e., $\text{PR}(X_{\text{FT}}) < \text{PR}(X_{\text{PT}})$, and that nearly all representational dimensions expressed post-fine-tuning are inherited from the pretraining state, i.e., $\text{ENSD}(X_{\text{PT}}, X_{\text{FT}}) \approx \text{PR}(X_{\text{FT}})$. The manifestation of this regime is more or less pronounced depending on the parameter we vary.

D.1. Experiments varying κ

The ResNet-18 architecture consists of an initial embedding layer followed by four stages of residual blocks, each containing two convolutional layers with identity skip connections. To induce imbalance across the network, we upscaled the embedding layer and the first three residual stages. In this experiment, we modify λ_{PT} during pretraining and leave the network unchanged during fine-tuning. In **Fig. 6** we observe that, for decreasing κ , the representation in the last layer looks like a signature of the pretraining-dependent rich regime described above. Furthermore, we observe that the overall dimensionality of the network decreases as a function of κ .

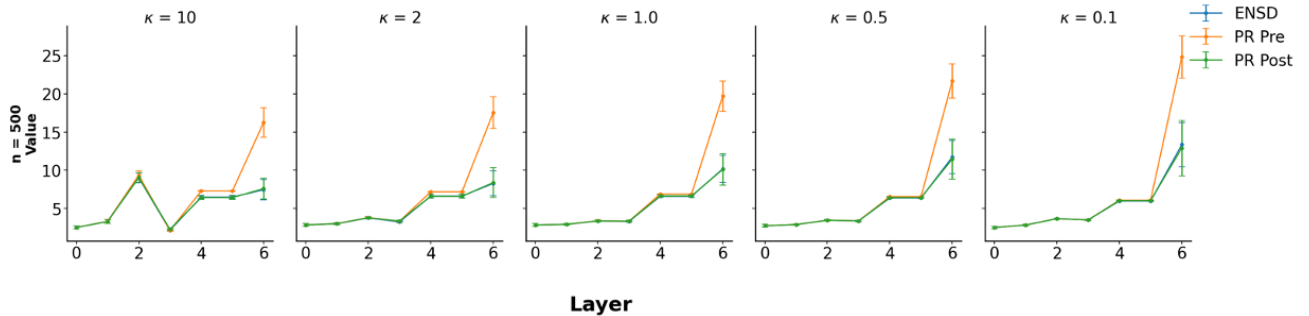


Figure 6. **ResNet experiments on CIFAR-100.** Resnet layers before and after fine-tuning (PR Pre and PR Post) as well as their ENSD as a function of the κ_{FT} re-initialization.

D.2. Experiments varying c_{PT}

To implement an equivalent notion of c_{PT} scaling in this architecture, we scale all network parameters by a constant factor κ . In this experiment, the overall scaling is applied during pretraining, while the network remains unchanged during

fine-tuning. In **Fig. 7** we observe that, for decreasing c_{PT} , the representation in the last layer looks like a signature of the pretraining-dependent rich regime described above.

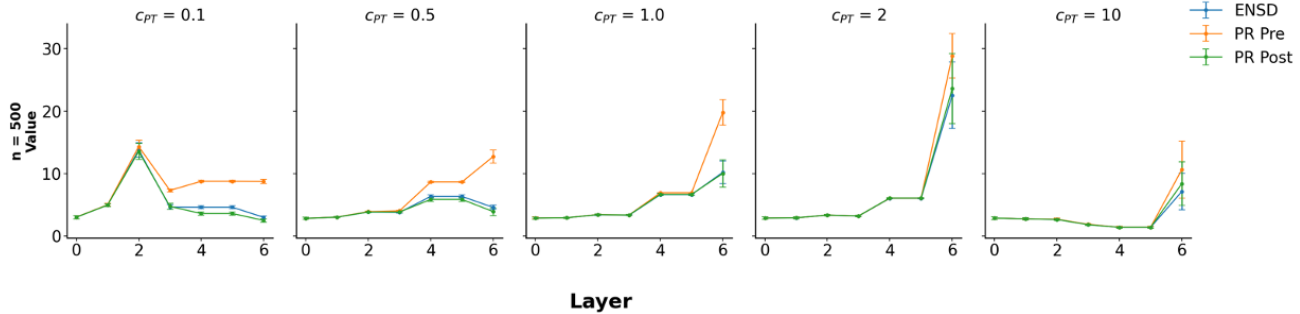


Figure 7. ResNet experiments on CIFAR-100. Resnet layers before and after fine-tuning (PR Pre and PR Post) as well as their ENSD as a function of the c_{PT} re-initialization.

D.3. Experiments varying γ_{FT}

To implement an equivalent notion of γ_{FT} rescaling in this architecture, we scale the last layer parameter. In this experiment, the overall scaling is applied during fine-tuning, while the network remains unchanged during pretraining. In **Fig. 8** we observe that, for decreasing γ_{FT} , the representation in the last layer looks like a signature of the pretraining-dependent rich regime described above.

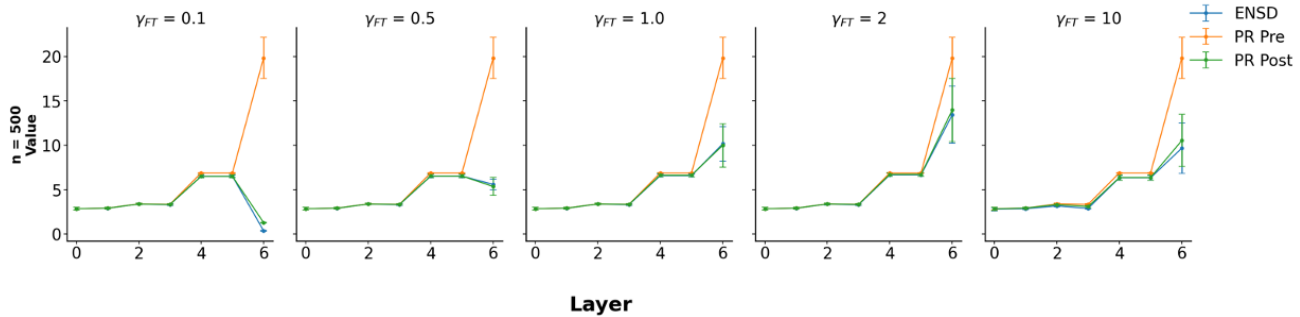


Figure 8. ResNet experiments on CIFAR-100. Resnet layers before and after fine-tuning (PR Pre and PR Post) as well as their ENSD as a function of the γ_{FT} re-initialization.

D.4. Experiments varying c_{FT}

For completeness, we include the heuristic proposed by (Lippl & Lindsey, 2024) for inducing a pretraining-dependent rich regime, which consists of rescaling all network weights by a constant $c_{FT} < 1$ during fine-tuning. As shown in **Fig. 9**, this heuristic is reported to improve performance relative to the baseline. The values found are not the same as the one reported in (Lippl & Lindsey, 2024) since the set of parameter used are different. In **Fig. 9** we observe that, for decreasing c_{FT} , the representation in the last layer looks like a signature of the pretraining-dependent rich regime described above.

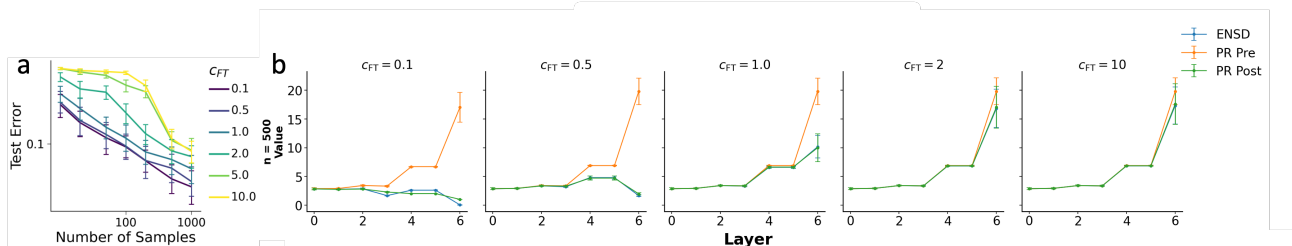


Figure 9. ResNet experiments on CIFAR-100. (a) Generalization performance as a function of the number of samples and initialization parameters. We vary c_{FT} . (b) Resnet layers before and after fine-tuning (PR Pre and PR Post) as well as their ENSD as a function of the γ_{FT} re-initialization.

D.5. Experiments discussion

First, our theoretical analysis is developed in a diagonal two-layer setting, whereas the ResNet architecture includes fully connected layers with residual connections and batch normalization, which may affect the applicability of our results. Moreover, extending the notion of balancedness to deeper networks remains an open problem, with only a few notable exceptions (e.g., (Kunin et al., 2024)). Second, our experiments do not explicitly control for sparsity levels or feature overlap, which may partially explain the observed performance discrepancies. We cautiously assume that the fine-tuning task exhibits lower sparsity than the pretraining task. Finally, our theoretical results are derived for linear networks, while ResNets are inherently nonlinear architectures. We leave a careful study of these parameters in practical networks to future work. Our theory serves to highlight the key initialization parameters that influence fine-tuning performance.

E. Implementation and Simulations

E.1. Figure 2

In the code we approximate

$$\text{PD} = \frac{\partial \log P(k, \beta_{FT})}{\partial \log \beta_{PT}} = \frac{\partial \log P}{\partial \log k} \cdot \frac{\partial \log k}{\partial \log \beta_{PT}} = \frac{\partial \log P}{\partial \log k} \cdot \frac{\partial k}{\partial \beta_{PT}} \cdot \frac{\beta_{PT}}{k} \quad (41)$$

$$= \left[\frac{1}{2} - \frac{\beta_{FT}}{\sqrt{k}} \cdot \frac{q'}{q} \right] \cdot \frac{\beta_{PT}}{k} \cdot \frac{\partial k}{\partial \beta_{PT}} \quad (42)$$

$$(43)$$

with

$$\frac{\partial k}{\partial \beta_{PT}} \approx \frac{k_+ - k_-}{2\epsilon}. \quad (44)$$

$$k_+ = 2(\lambda_{PT} + c_{PT}) \left(1 + \sqrt{1 + ((\beta_{PT} + \epsilon)/c_{PT})^2} \right) + \gamma_{FT}^2 \quad (45)$$

$$k_- = 2(\lambda_{PT} + c_{PT}) \left(1 + \sqrt{1 + ((\beta_{PT} - \epsilon)/c_{PT})^2} \right) + \gamma_{FT}^2 \quad (46)$$

E.2. Figure 3

E.2.1. SOLVING THE REPLICA FIXED POINT EQUATIONS NUMERICALLY

The RS order parameters are

$$p = \mathbb{E} \left[(\beta_{ft} - \hat{\beta}_{ft})^2 \right], \quad \chi = \theta_0 \mathbb{E} \left[\partial_y \hat{\beta}^{sc}(y; K, \theta) \right],$$

where the expectation is over (β_{ft}, K, v) with $y = \beta_{ft} + \sigma v$, $v \sim \mathcal{N}(0, 1)$, and $\sigma^2 = \theta_0 = (p + \sigma_0^2)/\alpha$.

The fixed-point closure is

$$\theta_0 = \delta(\sigma_0^2 + p), \quad \theta = \delta(\chi + \lambda),$$

with $\delta = 1/\alpha$, additive label-noise variance σ_0^2 (set to zero in the noiseless teacher setting), and an optional external ridge parameter λ .

These equations are solved iteratively for (θ_0, θ) at each α . In order to solve each equation, we need to evaluate to separate expectations.

The expectations defining p and χ are approximated by Monte-Carlo sampling. Given m i.i.d. samples $(\beta_{ft,i}, k_i, v_i)$, we form scalar observations

$$y_i = \beta_{ft,i} + \sqrt{\theta_0} v_i, \quad v_i \sim \mathcal{N}(0, 1).$$

For each y_i and penalty parameter k_i , the scalar estimator $\hat{\beta}_{ft,i}$ is given by the RS scalar denoiser

$$\hat{\beta}_{ft,i} = \hat{\beta}^{sc}(y_i; k_i, \theta) = \arg \min_{\beta \in \mathbb{R}} \left\{ \frac{(y_i - \beta)^2}{2\theta} + q_{k_i}(\beta) \right\}.$$

This scalar optimization balances fidelity to the noisy observation y_i against the implicit-bias penalty q_{k_i} , with θ controlling the strength of the quadratic term. For the q_k family considered here, the objective is strictly convex, so the minimizer is unique and can be computed reliably via a safeguarded Newton method.

At the scalar optimum, we also compute the local curvature

$$s_i^2 := \left(\frac{1}{\theta} + q''_{k_i}(\hat{\beta}_{\text{ft},i}) \right)^{-1},$$

where $\hat{\beta}_{\text{ft},i} = \hat{\beta}^{\text{sc}}(y_i; k_i, \theta)$ and $y_i = \beta_{\text{ft},i} + \sqrt{\theta_0} v_i$. This expression follows by implicit differentiation of the first-order optimality condition for the scalar denoiser:

$$0 = \frac{\hat{\beta}^{\text{sc}}(y; k, \theta) - y}{\theta} + q'_k(\hat{\beta}^{\text{sc}}(y; k, \theta)).$$

Differentiating both sides with respect to y gives

$$0 = \frac{1}{\theta} \left(\partial_y \hat{\beta}^{\text{sc}}(y; k, \theta) - 1 \right) + q''_k(\hat{\beta}^{\text{sc}}(y; k, \theta)) \partial_y \hat{\beta}^{\text{sc}}(y; k, \theta),$$

and therefore

$$\partial_y \hat{\beta}^{\text{sc}}(y; k, \theta) = \frac{1}{1 + \theta q''_k(\hat{\beta}^{\text{sc}}(y; k, \theta))} = \frac{s^2}{\theta}, \quad s^2 = \left(\frac{1}{\theta} + q''_k(\hat{\beta}^{\text{sc}}) \right)^{-1}.$$

We compute s_i^2 (equivalently $\partial_y \hat{\beta}^{\text{sc}}$) at the optimum because it provides a numerically stable evaluation of the susceptibility: it only involves the positive quantity $\frac{1}{\theta} + q''_{k_i}(\hat{\beta}_{\text{ft},i})$ (which is bounded away from zero under strict convexity), avoiding finite-difference approximations of $\partial_y \hat{\beta}^{\text{sc}}$ that can be noisy or ill-conditioned.

The Monte-Carlo estimates of the RS moments are then

$$\hat{p} = \frac{1}{m} \sum_{i=1}^m (\beta_{\text{ft},i} - \hat{\beta}_{\text{ft},i})^2, \quad \hat{\chi} = \theta_0 \cdot \frac{1}{m} \sum_{i=1}^m \partial_y \hat{\beta}^{\text{sc}}(y_i; k_i, \theta) = \theta_0 \cdot \frac{1}{m} \sum_{i=1}^m \frac{s_i^2}{\theta},$$

which are substituted into the fixed-point closure relations and iterated (with damping) until convergence.

When the penalty parameter k takes values in a finite set, the Monte-Carlo evaluation can be accelerated by grouping samples with identical k . In the PT→FT oracle considered here, k is deterministic conditional on PT activity: by construction (and because $\alpha_{\text{pt}} \geq 1$ in our setting), pretraining recovers the teacher exactly so each coordinate has $\hat{\beta}_{\text{pt},d} \in \{0, \pm 1/\sqrt{\rho_{\text{pt}}}\}$. Since k_d is a deterministic function of $\hat{\beta}_{\text{pt},d}$ and the initialization hyperparameters (cf. Eq. (15)), it follows that k_d can only take finitely many values (one for PT-inactive coordinates and one for PT-active coordinates, or more generally one per PT group if multiple groups are used). Importantly, while the proximal solution $\hat{\beta}^{\text{sc}}(y_i; k_i, \theta)$ depends on the sampled $\beta_{\text{ft},i}$ through y_i , the parameter k_i itself does not: it is fixed by the pretrained coordinate type (PT-active vs. PT-inactive). Therefore grouping by identical k is valid even though $\hat{\beta}_{\text{ft},i}$ varies across samples within a group.

E.2.2. FIXED-POINT ITERATION AND NUMERICAL STABILIZATION

Although the replica-symmetric fixed-point equations are theoretically well defined, naive numerical iteration can be unstable, especially near sharp transitions or in regimes with multiple admissible solutions. We therefore employ a damped fixed-point scheme with simple numerical safeguards to ensure stable and reproducible convergence.

Iteration variables. For a fixed inverse sample efficiency $\delta = 1/\alpha$, the solver iterates on the RS state variables (θ_0, g) . Given a current iterate, Monte-Carlo estimates of the RS moments \hat{p} and $\hat{\chi}$ are computed as described in Section 2 and used to form the updates

$$\theta_0^{\text{new}} = \sigma_0^2 + \delta \hat{p}, \quad g^{\text{new}} = \gamma_{\text{ext}} + \delta g \hat{\chi}.$$

A fixed point of this map defines the RS solution at the given α .

Damping. To suppress oscillations and divergence, the updates are applied with damping parameter $\lambda \in (0, 1]$:

$$\theta_0 \leftarrow (1 - \lambda)\theta_0 + \lambda\theta_0^{\text{new}}, \quad g \leftarrow (1 - \lambda)g + \lambda g^{\text{new}}.$$

Smaller values of λ slow convergence but substantially improve stability, particularly near phase transitions.

Positivity constraints. The RS variables are constrained to remain in their admissible domains by enforcing

$$\theta_0 \geq \sigma_0^2, \quad g \geq g_{\min},$$

where $g_{\min} > 0$ is a small numerical floor. These constraints prevent degeneracy in the scalar denoiser and curvature evaluation and act purely as numerical safeguards. In practice, we pick $g_{\min} = 10^{-14}$.

Convergence criteria. Convergence is assessed using the maximum absolute residual

$$\text{res} = \max\{|\theta_0^{\text{new}} - \theta_0|, |g^{\text{new}} - g|\}.$$

The iteration terminates when $\text{res} < \text{tol}$ or when a preset iteration limit is reached.

E.2.3. STABILIZATION ACROSS SAMPLE EFFICIENCIES

In addition to within- α stabilization, the RS fixed-point equations may admit multiple stable solutions as the sample efficiency α varies. To robustly track solutions across α , we use continuation with warm starts and a simple branch-selection rule.

Forward/backward continuation in α . Given a grid of sample efficiencies $\{\alpha_j\}$ (equivalently $\delta_j = 1/\alpha_j$), we solve the fixed-point equations sequentially in two passes. In the forward pass, solutions at α_j are initialized using the converged state from α_{j-1} ; in the backward pass, the grid is traversed in reverse order, initializing from α_{j+1} . This bidirectional continuation helps detect multistability and reduces sensitivity to initialization.

We explicitly verify that the forward and backward continuations converge to consistent solutions across the entire grid. For each α_j , we compare the converged forward and backward fixed points and observe no evidence of multistability. Quantitatively, the median branch mismatch $\|\theta_{\text{fwd}} - \theta_{\text{bwd}}\|$ is $\sim 1.5 \times 10^{-7}$ (with the 95th percentile below 2×10^{-6}), and the corresponding fixed-point residuals are of order 10^{-7} – 10^{-6} . The resulting Monte-Carlo estimates of p and χ differ by less than 1.5% in median and 2.5% at the 95th percentile, well within the intrinsic sampling error.

In addition, the implementation includes an automated reliability score that flags numerical instabilities; no runs failed to converge or exhibited exploding behavior across all sweeps. A small MSE floor ($\sim 10^{-12}$) is used to prevent numerical issues in the high-sample-efficiency regime, where such instabilities are known to arise. Taken together, these checks confirm that the fixed-point solutions are robust, path-independent, and insensitive to the direction of continuation in α .

Warm starts. At each α_j , the fixed-point iteration is warm-started from the nearest converged solution along the continuation path, rather than from a generic initialization. This reduces the number of iterations required for convergence.

Branch selection rule. Forward and backward continuation may converge to different fixed points at the same α , reflecting genuine RS multistability. In such cases, we select the branch with smaller predicted MSE as the reported solution. The discrepancy between forward and backward solutions is retained as a diagnostic of numerical sensitivity.

E.2.4. DIAGNOSTICS AND RELIABILITY CHECKS

To assess the reliability of numerical RS solutions, we record diagnostics that quantify fixed-point convergence, multistability across continuation paths, and Monte-Carlo uncertainty.

Residual checks. For each α , convergence is monitored using the fixed-point residual

$$\text{res} = \max\{|\theta_0^{\text{new}} - \theta_0|, |g^{\text{new}} - g|\}.$$

Solutions with $\text{res} > \text{tol}$ are considered unconverged and flagged as unreliable.

Branch mismatch. Let $\text{MSE}_{\text{fwd}}(\alpha)$ and $\text{MSE}_{\text{bwd}}(\alpha)$ denote the RS predictions obtained from forward and backward continuation, respectively. We quantify branch disagreement via

$$\Delta_{\text{branch}}(\alpha) = \left| 10 \log_{10}(\text{MSE}_{\text{fwd}}(\alpha)) - 10 \log_{10}(\text{MSE}_{\text{bwd}}(\alpha)) \right|.$$

Large values indicate RS multistability or sensitivity to initialization.

Monte-Carlo uncertainty. Let

$$e_i^2 = \left(\beta_{\text{ft},i} - \hat{\beta}_{\text{ft},i} \right)^2.$$

The Monte-Carlo estimate

$$\widehat{\text{MSE}} = \frac{1}{m} \sum_{i=1}^m e_i^2$$

is assigned a standard error $\text{SE}(\widehat{\text{MSE}})$, computed using batch-means estimation. Uncertainty on the log scale is approximated via the delta method,

$$\text{SE}_{\text{dB}} \approx \frac{10}{\ln 10} \frac{\text{SE}(\widehat{\text{MSE}})}{\max\{\widehat{\text{MSE}}, \varepsilon\}},$$

with a small floor $\varepsilon > 0$ to avoid numerical blow-up.

Failure indicators. A solution at α is flagged as unreliable if any of the following occur:

- $\text{res} > \text{tol}$: the fixed-point residual exceeds the prescribed tolerance. In all experiments, the residual remained strictly below $\text{tol} = 10^{-10}$, with a maximal observed value of approximately 9.9×10^{-7} .
- $\Delta_{\text{branch}}(\alpha)$ exceeds a prescribed threshold: the mismatch between forward and backward continuation branches becomes large. Across all sweeps, the maximal observed branch mismatch (Δ_{branch} , measured in dB) was approximately 3.6×10^{-4} dB, occurring in the most challenging low- α regimes, and is negligible relative to the reported MSE effects.
- SE_{dB} is comparable to or larger than the reported effect size: the Monte Carlo standard error of the predicted MSE (in dB) becomes large. In practice, SE_{dB} was capped by a numerical floor and remained below approximately 0.07 dB even in the low- α regime, ensuring that uncertainty in the RS predictions remains well controlled as $\text{MSE} \rightarrow 0$.

These indicators are retained alongside RS predictions to identify unstable or poorly resolved regions. In the current experimental setups, no solutions exceeded these reliability thresholds.

The consistently small values of all failure indicators can be attributed to (i) strict convergence criteria combined with conservative damping and a large iteration budget, (ii) the absence of detectable multistability in the explored parameter regimes, as evidenced by near-identical forward and backward continuations, and (iii) explicit slope capping in the dB-scale error estimation, which prevents numerical amplification of Monte Carlo uncertainty at very small MSE.

E.2.5. PARAMETER SWEEPS AND CURVE GENERATION

All replica-theory curves are generated by solving the RS fixed-point equations over a dense grid of sample efficiencies α , mirroring the structure of the corresponding empirical experiments.

Numerical parameters. Replica fixed-point equations are solved using Monte-Carlo approximation with $m = 80,000$ samples per α . Fixed-point iteration uses damping factor 0.25, convergence tolerance $\text{tol} = 10^{-6}$, and a maximum of 900 iterations per α . A small external ridge parameter $\gamma_{\text{ext}} = 10^{-6}$ is included to improve numerical stability. All runs use a single random seed.

Parameter sweeps. For each experiment, a baseline configuration is evaluated together with one-dimensional sweeps over individual hyperparameters, with all remaining parameters held fixed. Baseline values are excluded from sweep lists to avoid duplicate runs. Each parameter configuration produces a full generalization curve indexed by α .

Parallelization and curve assembly. To increase parallelism, the α -grid may be partitioned into contiguous chunks, with each job solving the RS equations on a subset of α values for a fixed parameter configuration. Results from all chunks are concatenated to form the final curve, which is saved together with per- α diagnostics and metadata.

E.2.6. DIAGONAL NETWORK EXPERIMENTS (EMPIRICAL SETUP)

This section specifies the empirical diagonal-network experiments used to compare finite-dimensional training with the replica-symmetric predictions. All experiments use diagonal linear networks trained by gradient flow and are averaged over multiple random seeds.

Global settings. Unless stated otherwise, all experiments use the following hyperparameters:

Parameter	Value
Input dimension d	5000
Test samples	10,000
Learning rate	0.5
Max epochs	5×10^6
Convergence threshold	10^{-4}
Data scale $\alpha = n/d$	11 values in $[0.01, 0.5]$
Random seeds	14 (seeds 6–19)
Teacher signal scale a_{PT}	1.0
Pretraining sparsity ρ_{PT}	0.1

Mean squared error is evaluated on an independent test set after convergence.

Task parameterization and overlap. Fine-tuning task structure is specified by $(\rho_{FT}^{\text{shared}}, \rho_{FT}^{\text{new}})$ as in Eq. (11), with total fine-tuning sparsity

$$\rho_{FT} := \rho_{FT}^{\text{shared}} + \rho_{FT}^{\text{new}}.$$

For convenience, we additionally report the *overlap fraction*

$$\omega := \frac{\rho_{FT}^{\text{shared}}}{\rho_{FT}^{\text{shared}} + \rho_{FT}^{\text{new}}} \in [0, 1],$$

so that, for a fixed ρ_{FT} , sweeping ω corresponds to setting $\rho_{FT}^{\text{shared}} = \omega \rho_{FT}$ and $\rho_{FT}^{\text{new}} = (1 - \omega) \rho_{FT}$.

Pretrain–fine-tune protocol. For pretrain–fine-tune (PT+FT) experiments, fine-tuning is initialized from an analytically constructed infinite-pretraining state determined by the pretraining teacher β_{PT} and homogeneous parameters (c_{PT}, λ_{PT}) . Here we assume $\alpha_{PT} \geq 1$ so that pretraining perfectly recovers the ground truth β_{PT} . At the start of fine-tuning, a reinitialization scale γ_{FT} is applied to set $\beta(0) \approx 0$ while preserving the coordinate-wise richness structure.

Experiment 1: Benefit from existing features. Fixed parameters:

$$\rho_{PT} = 0.1, \quad \rho_{FT} = \rho_{FT}^{\text{shared}} + \rho_{FT}^{\text{new}} = 0.1.$$

Baseline:

$$\omega = 0.5 \text{ (i.e., } \rho_{FT}^{\text{shared}} = \rho_{FT}^{\text{new}} = 0.05), \quad c_{PT} = 10^{-3}, \quad \lambda_{PT} = 0, \quad \gamma_{FT} = 0.$$

Swept parameters:

Parameter	Values
Overlap fraction ω	$\{0, 0.5, 1\}$
c_{PT}	$\{10^{-6}, 10^{-3}, 1\}$
λ_{PT}	$\{-10^{-3}, -0.99 \cdot 10^{-3}, 0, 0.99 \cdot 10^{-3}\}$
γ_{FT}	$\{0, 1, 10\}$

Experiment 2: Learning new features. Fixed parameters:

$$\rho_{PT} = 0.1, \quad \rho_{FT}^{\text{shared}} = 0 \text{ (equivalently } \omega = 0).$$

Swept parameters:

Parameter	Values
ρ_{FT}^{new} ($\rho_{FT} = \rho_{FT}^{\text{new}}$ since $\rho_{FT}^{\text{shared}} = 0$)	$\{0.1, 0.9\}$
$c_{PT}, \lambda_{PT}, \gamma_{FT}$	same as Experiment 1

Experiment 3: Nested feature regime. Fixed parameters:

$$\rho_{PT} = 0.1.$$

Swept parameters:

Parameter	Values
Overlap fraction ω	$\{0, 1\}$
ρ_{FT}	$\{0.01, 0.04\}$
Implied $(\rho_{FT}^{\text{shared}}, \rho_{FT}^{\text{new}})$	$\omega = 1 : (\rho_{FT}^{\text{shared}}, \rho_{FT}^{\text{new}}) = (\rho_{FT}, 0)$ $\omega = 0 : (\rho_{FT}^{\text{shared}}, \rho_{FT}^{\text{new}}) = (0, \rho_{FT})$
$c_{PT}, \lambda_{PT}, \gamma_{FT}$	same as Experiment 1

Experiment 4: Single-task learning (SLT). In this setting, the network is trained from scratch without pretraining. We generate a single sparse task with sparsity ρ (denoted ρ_{PT} for notational consistency).

Swept parameters:

Parameter	Values
Task sparsity ρ (denoted ρ_{PT})	$\{0.01, 0.04, 0.1, 0.9\}$
c_{PT}	$\{10^{-6}, 10^{-3}, 1\}$
λ_{PT}	$\{0, -c_{PT}, -0.99c_{PT}, 0.99c_{PT}\}$

Mapping to replica curves. Empirical results are compared to replica-symmetric predictions by mapping the initialization at the start of fine-tuning to the replica penalty parameter

$$k_i = 4c_{FT,i}^2,$$

and solving the associated fixed-point equations for each data scale α .

Code. The experiments and replica curves are generated using:

- `ptft_empirical_finetune_df.py`
- `ptft_replica_qk.py`
- `compute_emp_curves_worker_exp[1--4].py`
- `ExperimentSetup.md`

E.3. Figure 4

All experiments are performed using ResNet-18. Each plot is based on 30 random seeds, with the mean performance shown and standard errors represented as error bars. The network is pre-trained on 49,000 samples until the loss reaches 0.01. During fine-tuning, the number of samples is varied as indicated in the figure, using a loss threshold of 0.0001. For the corresponding ENSD experiments, we use 500 samples.